



VIBROACOUSTIC RESPONSE OF A THIN CYLINDRICAL SHELL EXCITED BY A TURBULENT INTERNAL FLOW: COMPARISON BETWEEN NUMERICAL PREDICTION AND EXPERIMENTATION

C. DURANT AND G. ROBERT

*Laboratoire de Mécanique des Fluides et d'Acoustique, UMR CNRS 5509,
École Centrale de Lyon, BP 163-69131 Ecully Cedex, France*

AND

P. J. T. FILIPPI, P.-O. MATTEI

*Laboratoire de Mécanique et d'Acoustique, UPR CNRS 7051, 31, chemin Joseph-Aiguier
13042, Marseille Cedex 20, France*

(Received 29 March 1999, and in final form 26 July 1999)

The main aspect of this work is to establish a comparison between the measured and the modelled vibroacoustic response of a thin cylindrical pipe excited by a turbulent internal flow. The first part presents the experiment. A Corcos-like model of the wall pressure fluctuation is proposed. The vibroacoustic response of the shell is measured. A numerical method based on a boundary integral formulation and a matched asymptotic expansion is developed. Computed spectral densities of the velocity of and acoustic sound pressure radiated by the shell are compared with experimental results. The comparison shows an agreement within a few decibels.

© 2000 Academic Press

1. INTRODUCTION

Turbulent boundary excitation of a structure is a phenomenon of great practical importance, particularly in the field of high-speed transport technology. The problem involves the coupling of structural and fluid vibrations. This aspect has assumed increased importance because of the emergence of problems of dense fluid loading in the field of marine acoustics and fluid machinery. While many studies have been published on the problem of a thin elastic plate (or membrane) excited by a turbulent boundary layer, much less is known about the vibroacoustic response of a shell. This is mainly because during the last decades the turbulent flow had not been considered as a major source of noise in regards to other phenomena such as vortex shedding, propagating plane waves and acoustic high order modes inside the

pipe or mechanical excitation [1]. These sources are now understood and the turbulent excitation becomes again a field of research. To our knowledge, the first attempt to make a realistic comparison of measured and predicted pipe vibration was made by Clinch [2]; the hypotheses made for the theoretical model (continuous resonance response) and the results obtained are valid at high frequencies. But only the first resonance frequencies of the shell make a significant contribution to the sound radiated by the shell. A more recent work was done by Horáček [3]. In this work, similar to ours, the author studied the dynamic response, using normal mode approach, of a thin shell (using the Goldenveizer–Novozhilov linear theory) in vacuum, simply supported on its boundary. The shell is excited by a wall pressure field due to internal turbulent flow of air. Also, in the book by Blake [4] one can find an extensive amount of references and the basic explanation of flow noise mechanism and sound radiation by pipes.

This study deals with the particular case of a finite thin cylindrical pipe excited by a fully developed turbulent internal flow. The main hypotheses made here are: (1) the shell vibration has no influence on the structure of the flow, this means that the turbulent wall pressure fluctuation acts on the shell as a given random process; (2) the flow speed is small enough to be neglected in the wave propagation equation; and (3) the effect of the fluid-loading on the shell motion can be considered as a small perturbation.

The assumption of non-influence of the shell vibration on the wall pressure field is usually admitted for flow-induced noise and vibration phenomena. It is the only way to measure the wall pressure field on a rigid structure and consider that this pressure field is the same as on the vibrating structure. Here we verify this assumption by comparing the amplitude of the vibration with a characteristic dimension of the flow: the viscous sub-layer thickness δ_* . Moreover, the acoustic pressure radiated by the shell is lower than the turbulent pressure to affect the wall pressure field.

In the first section of this paper, the experimental facility is detailed. Then, in the second section, the measured characteristics of the wall pressure field are presented. The power spectral density, the correlation lengths and the convection velocity are included in a Corcos-like model for the cross-spectrum of the wall pressure field. This model is directly used for the numerical predictions. The third part of this paper deals with the theoretical model of the vibroacoustic response of the shell to a random excitation. This response is characterized by a cross-power spectral density, given as a two-dimensional integral over the domain occupied by the structure of a product between the response of the structure to a point unit force, its conjugate and the cross-spectrum density of the excitation force. This response is estimated by a method that combines the resolution of the exact equations (by a boundary element method) with an asymptotic expansion which takes into account the low density of the interior fluid with respect to the shell density. But this problem displays some of the features of a singular perturbation problem. It is common sense that the presence of a fluid like air inside the shell does not change the physical properties of the shell. So one can define ε as the ratio of the fluid density to the shell surface density. ε is a small parameter in our problem. The Green representation of the internal acoustic pressure is not defined for the cut-off

frequencies of the duct. A regular solution is obtained in the form of a matched asymptotic expansion [5]. Similar methods [6, 7] have been used for membrane or elastic targets. The last part of this paper presents a comparison between the theoretical and experimental normal velocities of the shell. The results agree very well (within a few percent). Some comments conclude the paper.

2. EXPERIMENTAL ARRANGEMENT

Measurements were made in the wind tunnel of the LMFA of Ecole Centrale de Lyon. The tunnel was specially designed to minimize acoustic contamination by upstream machinery and ambient noise. The primary air is first propelled to a slow speed by a centrifugal blower located in a room mechanically isolated from the rest of the building for vibration reasons. Acoustic mufflers are located both upstream and downstream of the blower in order to reduce background noise. Then the air passes through an acceleration section made up of a honeycomb section, two sections of grids and a contraction with an area ratio of four. Finally, the air arrives in the last assembly, which is inside a large anechoic chamber. This last assembly, shown schematically in Figure 1, is made from interchangeable sections of steel tubing with an internal diameter of 125 mm, a wall thickness of 7.5 mm and an overall length of about 10.5 m. At the upstream end of the pipe, a honeycomb and a little step accelerates the formation of the fully developed turbulent flow. The bores of the various pipe sections are accurately matched, and mating pipe sections joined by flanges, so that no disturbances due to discontinuities at the joints were introduced. The pipe rig is guided over its entire length by a series of supports. The test section is connected to the rest of the pipe at its downstream and upstream ends by elastic joints and supported by elastic supports, so that the test section is effectively isolated from the vibration of the rest of the pipe. The measurements confirmed a difference of 30 dB between the vibration level of the test section and the rest of the pipe.

The test section is mounted 5.5 m (≈ 45 pipe diameters) downstream of the pipe entrance to achieve homogeneity and stationarity for the flow in the region of the test section.

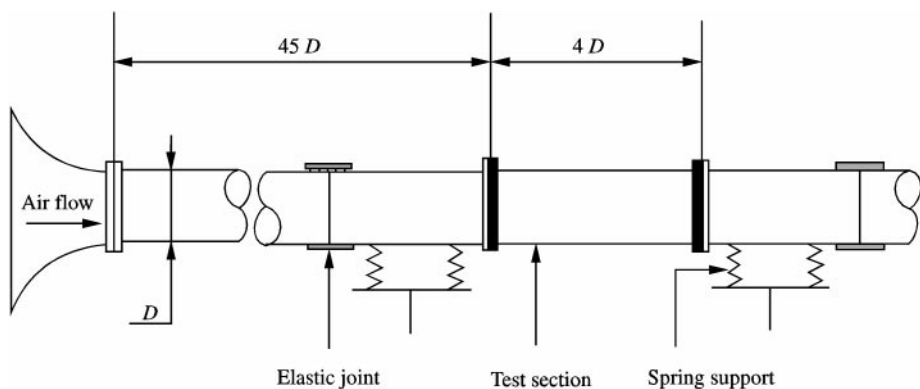


Figure 1. Pipe rig facility.

The wall acceleration and the external acoustic pressure were measured for a 0.46 m long and 0.5 mm wall thickness test section. This thin cylindrical shell was manufactured from a plane sheet steel, rolled, carefully soldered and heat treated. The acceleration measurements were made both with very light Brüel and Kjær 4374 (0.65 g) piezoelectric accelerometers and a laser vibrometer POLYTEC (OFV-302). As the surface mass of the pipe test section is low (3.9 kg/m²), the accelerometers introduce a non-negligible added mass effect which shifts the modal frequencies of the structure. The non-contact laser measurements were made to obtain a better agreement with the calculated vibroacoustic response. The external acoustic pressure was measured with Brüel and Kjær 4135 (6.35 mm external diameter) microphones at distances from the pipe wall ranging from 5 mm to 1 m.

It was assumed that the vibrations of the test section did not modify the turbulent wall pressure field so that the statistical properties of the wall pressure were measured on the surface of a rigid section (7.5 mm thickness). This assumption was based on the comparison of the root-mean-square (r.m.s.) value of the displacement of the test section ($(\overline{u_r^2})^{1/2}$) with respect to the viscous sub-layer thickness of the flow, δ_τ . The viscous sub-layer thickness was estimated from the formula given by Schlichting [8]

$$\delta_\tau \simeq 5\nu/u_\tau, \quad (1)$$

where u_τ is the friction velocity and ν the kinematic viscosity. In the worst case, for a mean flow velocity $U_0 \simeq 120$ m/s, it was found that $(\overline{u_r^2})^{1/2} \simeq 0.26$ μm and $\delta_\tau \simeq 12.5$ μm . The turbulent pressure sources are actually located beyond the viscous sub-layer and as the r.m.s. value of the displacement was found to be much lower than the viscous sub-layer thickness, we concluded that the vibrations of the test section did not influence the turbulent wall pressure field.

To measure the turbulent wall pressure, the thin test section was replaced by a rigid section equipped with nine flush-mounted Brüel and Kjær 4135 (6.35 mm external diameter) microphones. By referring to the assumption of the separation of the space variables for the cross-spectra model [9], two series of measurements were made. First, the nine microphones were located along a line in the longitudinal direction (see Figure 2(a)); intervals varied from 8 to 144 mm with respect to the reference microphone. Next, the nine microphones were located on a circumference (see Figure 2(b)) with angular separations varying from 8 to 120°.

The centerline velocity of the flow inside the pipe varied up to 120 m/s. Flow velocity measurements were made with a Dantec 55P11 hot-wire probe. The probe support was guided in the direction transverse to the flow. By translating the probe to various known locations along the pipe diameter, the velocity profile was recorded.

The friction velocity was calculated from the measurement of the static pressure at six locations distributed along the pipe.

All measurements (friction velocity, velocity profile, wall pressure, acceleration response and acoustic pressure) were made for four centerline reference velocities: 60, 80, 100 and 120 m/s.

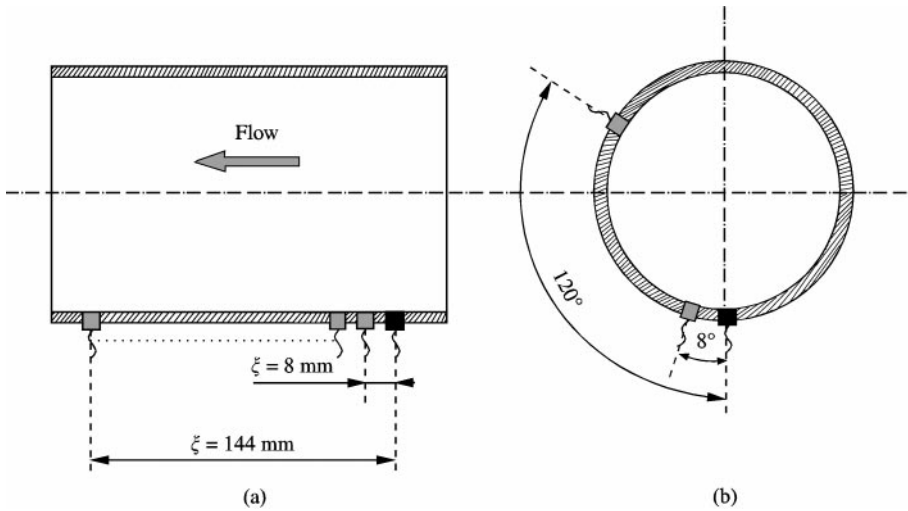


Figure 2. Longitudinal (a) and circumferential (b) positioning of the microphones.

All signals were processed by an HP 3566A/67A analyzer (16 tracks, 12.8 kHz bandwidth). Wall pressure and acoustic signals were averaged over 1000 realizations, so that random errors in the power spectral density were of the order of 3% or 0.25 dB [10]. Acceleration signals were averaged over 100 realizations only but the random errors were still less than 1 dB.

3. EXPERIMENTAL RESULTS AND DISCUSSION

3.1. MEAN FLOW VELOCITY

To confirm that the turbulent flow in the pipe test section was fully developed, a number of preliminary experiments were performed. First, the mean velocity profile was measured by using a hot-wire probe. Second, the friction velocity u_τ and the resistance coefficient λ were determined from the measurements of the static pressure along the pipe.

Figure 3 shows a typical velocity profile, normalized by the centerline pipe flow velocity U_0 . In this figure, the experimental data are compared with the empirical velocity distribution law proposed by Schlichting [8] for fully developed turbulent flow in a smooth-walled pipe,

$$u/U_0 = (2y/D)^{1/n}, \quad (2)$$

where u is the local velocity at a distance y from the wall and D is the pipe diameter. The exponent n varies slightly with the Reynolds number $\mathcal{R}_0 = U_0 D/\nu$. For the particular Reynolds number $\mathcal{R}_0 = 8.9 \times 10^5$, Schlichting gives an exponent $n = 8.2$. A good agreement is observed in Figure 3(a) between the measurements and the power law. Similar results have been obtained for other Reynolds numbers ranging from 5.3×10^5 to 1.1×10^6 . It must be noted here that the power law is only an

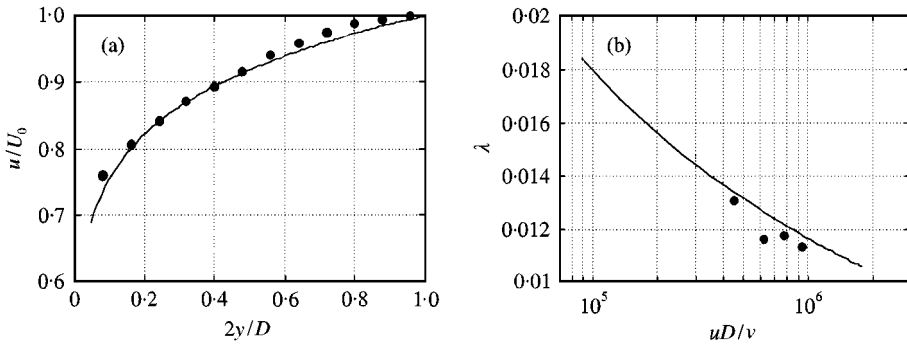


Figure 3. Typical mean velocity profile ($\mathcal{R}_o = 8.9 \times 10^5$): (a) and Prandtl's law (b). ●, experimental data; (a) —, power law ($n = 8.2$); (b) —, Prandtl's law.

approximation of the mean flow profile which is not valid in the central region of the flow. However, the good agreement between the measurements and this law for a large range of values of y is generally accepted as a criterion of a fully developed turbulent pipe flow.

Another criterion proposed by Sabot [11] is the verification of Prandtl's universal law of friction,

$$\frac{1}{\sqrt{\lambda}} = 2 \log \left(\frac{\bar{u}D}{\nu} \sqrt{\lambda} \right) - 0.8, \quad (3)$$

where \bar{u} is the mean flow velocity and $\lambda = 8(u_\tau/\bar{u})^2$. A good agreement is again found between the experimental data and this law (see Figure 3(b)) and confirms that the flow be considered as fully developed.

3.2. POWER SPECTRAL DENSITY

The power spectral density of the wall pressure fluctuations $\Phi_p^0(f)$ is displayed in Figure 4 for the four centerline reference velocities as a function of the frequency f . The analysis was limited to the frequency range $[0, 3200 \text{ Hz}]$ which is sufficient in view of the computation of the vibroacoustic response of the pipe test section. Two spectral regions are of special interest. In the low-frequency range, below 200 Hz, some peaks appear as observed by other investigators [12–14]. These peaks have been identified as longitudinal acoustic modes that occur in the pipe between the upstream convergent and the exit section. These modes are excited by the turbulence inside the pipe. Under the idealized conditions of pipe flow with a constant velocity profile, the frequency of these modes is given by the relation [15]

$$f_m = m(c_i/2L_p)(1 - M^2)^{1/2}, \quad (4)$$

where m is an integer, c_i the sound speed, L_p the total pipe length ($L_p \simeq 10.5 \text{ m}$) and M the flow Mach number. Figure 4 shows the first mode around 15 Hz and its

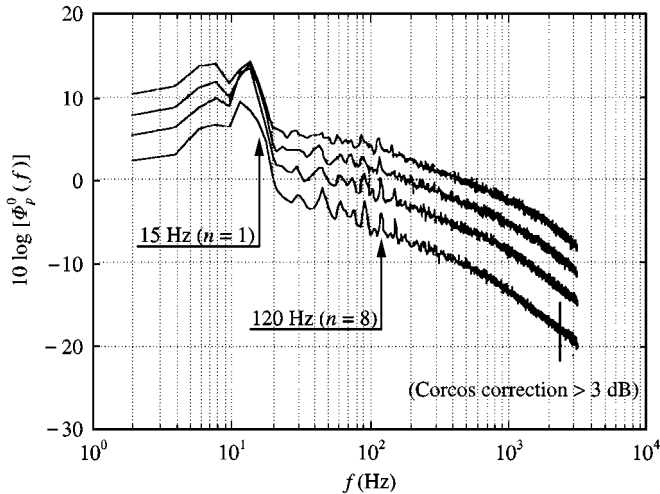


Figure 4. Wall pressure power spectral density for 60, 80, 100 and 120 m/s.

harmonics. The slight decrease of the frequencies with increasing Mach number is also observed for the harmonic $m - 8$ (120 Hz). Note that the higher acoustic modes do not contribute to the wall pressure field (no peak above the acoustic cut-off frequency of the pipe ≈ 1600 Hz). Therefore, the wall pressure exhibits an acoustic component and a turbulent component. To have further information on the turbulent wall pressure field, some authors have reported signal processing methods to cancel the acoustic component from the power spectral density of the wall pressure fluctuations. These methods are based on the principle that the acoustic field is more coherent than the turbulence in the spanwise direction and can be cancelled either by a temporal subtraction method [16–19] or by a coherent output power technique [20]. With regard to the computation of the vibroacoustic response of the pipe test section, the two components of the wall pressure are needed, thus no noise cancellation techniques have been applied here. In addition, the first structural mode of the pipe test section is around 570 Hz and above this frequency the turbulent component is largely predominant.

In the high-frequency range, the decrease of the power spectral density is accentuated by the size effect of the microphone. In fact, spatial averaging over the face of the microphone low-pass filters the signal and, as a result, small microphones are more accurate than large microphones in measuring wall pressure fluctuations. This problem of spatial resolution has been approached by many authors [9, 21–25] and the Corcos theory is most commonly used to correct experimental wall pressure data. With the assumption of a uniform sensitivity distribution over the face of the pressure sensor, Corcos showed that the ratio of the measured power spectral density to its true value depends only upon the quantity $\omega r/U_c$ where r is the microphone radius and U_c the convection speed. In Figure 4, the dash indicates the frequency limit beyond which the spectral level is assumed to be attenuated more than 3 dB for $U_0 = 60$ m/s. This frequency limit is higher than 3200 Hz for the other velocities.

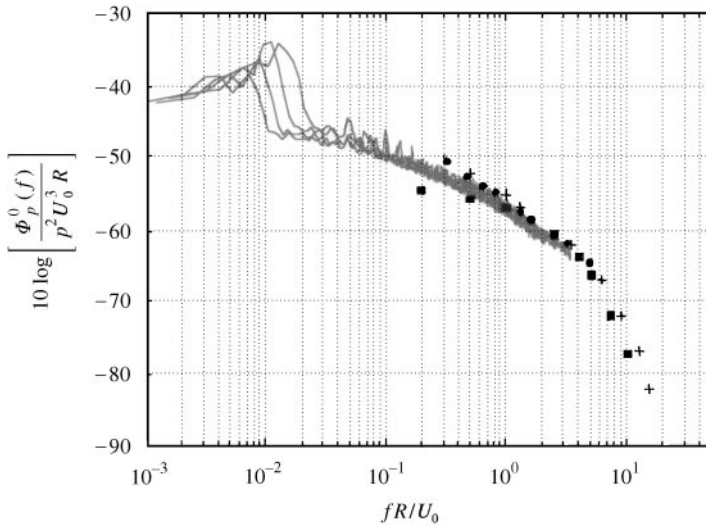


Figure 5. Non-dimensional wall pressure power spectral density scaled on outer variables for 60, 80, 100 and 120 m/s, ■, Bakewell *et al.*; +, Clinch; ●, Agarwal.

In Figure 5, the measured spectral data with no Corcos correction are displayed with the outer variable scaling in the form

$$\Phi_p^0(f)/\rho_i^2 U_0^3 R \text{ versus } fR/U_0, \quad (5)$$

where R is the pipe radius and ρ_i the air density. The scaling law based on the outer variables is more efficient for the low-frequency domain (our range of interest). The scaling laws based on the mixed or inner variable do not provide any collapse of the experimental data. A fairly good agreement is observed between the power spectral densities measured at 60, 80, 100 and 120 m/s. Some works [26, 27] have already demonstrated the effectiveness of this scaling law to collapse data in the low-frequency range. The non-dimensionalized scaling law has two advantages. First, it allows comparisons with results of other investigators. Thus, in Figure 5, the measured spectral data are compared with a set of measurements by Bakewell *et al.* [28] (air flow), Clinch [14] (water flow) and Agarwal [29] (air flow). Though there are differences in investigation characteristics (pipe radius, velocity, pressure sensor, etc.), a good agreement is found and confirms the validity of the present measurements. Second, an analytical expression of the non-dimensional wall pressure power spectral density can be deduced from this representation. This extends the excitation database to any particular flow velocity. This work is not presented here because the vibroacoustic response database, and hence the numerical predictions, is limited to the four reference flow velocities defined above.

3.3. CROSS-SPECTRAL FEATURES OF THE WALL PRESSURE FIELD

A model of the cross-spectrum of the fluctuating pressure field $\phi_p(\xi, \eta, f)$ is needed as an input to the numerical predictions. The classical fluctuating pressure

models at the surface of a rigid body are due to Chase [30] and Corcos [21]. For a more complete explanation, see recent review papers by Leehey [31], Bull [32] or the book by Blake [4]. A numerical comparison of the various turbulent boundary pressure models is presented by Graham [33]. In our study, the cross-spectrum was analyzed according to Corcos' approach [9, 21],

$$\Phi_p(\xi, \eta, f) = \Phi_p^0(f)C(\xi, \eta, f)\exp(i\theta(\xi, f)), \tag{6}$$

where $\Phi_p^0(f) = \Phi_p(0, 0, f)$. $\theta(\xi, f)$ is the phase function which depends only on the longitudinal separation ξ because of the convection phenomena and $C(\xi, \eta, f)$ describes, as a function of frequency, the decay of the coherence of the pressure field as it is convected over a longitudinal distance ξ and a circumferential distance η . The space variables separation hypothesis, though discussed by some authors [34], permits simplification:

$$C(\xi, \eta, f) = A(\xi, f)B(\eta, f). \tag{7}$$

The coherence has been measured for the four reference velocities and for a wide range of streamwise and spanwise spacings ($0.13 \leq \xi/R \leq 2.3$ and $0.14 \leq \eta/R \leq 2.1$). The results are displayed in Figure 6 for two frequencies. A number of interesting features are readily apparent. The first observation is that the spanwise coherence $B(\eta, f)$ is much smaller than the streamwise coherence $A(\xi, f)$. The turbulent structures are actually convected in the flow direction and remain coherent over long distances whereas the convection phenomenon does not exist in the spanwise direction. Second, the decay rate is not constant but slowly increases with frequency both for streamwise and spanwise coherence. Third, the shape of the evolution of the coherence versus the separation suggests an approximation by

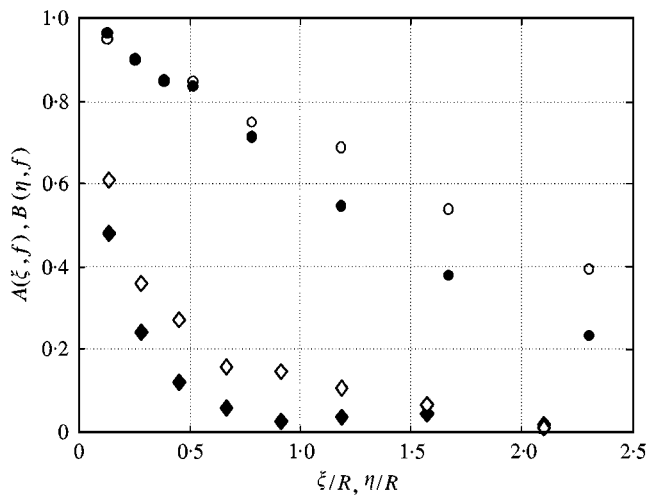


Figure 6. Streamwise and spanwise coherence for 100 m/s and two frequencies (660 and 1200 Hz). Streamwise: ○, 660 Hz; ●, 1200 Hz. Spanwise: ◇, 660 Hz; ◆, 1200 Hz.

a decreasing exponential function as accepted by many authors,

$$A(\xi, f) = \exp\left(\frac{-|\xi|}{L_\xi(f)}\right), \quad B(\eta, f) = \exp\left(\frac{-|\eta|}{L_\eta(f)}\right), \quad (8, 9)$$

where $L_\xi(f)$ and $L_\eta(f)$ are respectively the longitudinal and circumferential correlation lengths (integral scales). These lengths are frequency dependent and have been computed for each frequency step (see Figure 7). In the low-frequency range, the behavior of the longitudinal correlation length is rather perturbed because this zone is essentially governed by the acoustic component of the pressure field and the exponential fitting is no more valid. After this zone, $L_\xi(f)$ decreases slowly with frequency and thus expresses the fact that the smaller flow structures associated with higher frequencies remain coherent over shorter distances than larger turbulent structures. The computation of the circumferential correlation length is limited in high frequency because the coherence decreases rapidly with frequency and there are no more enough significant points for the exponential fitting. In the frequency band [500, 1500 Hz], the correlation length ratio $L_\xi(f)/L_\eta(f)$ is about 5 which is in good agreement with the results of Clinch [14]. Similar computations have been made for other flow velocities and it was found that the correlation lengths decrease slowly with decreasing flow velocity. It must be noted that for the comparison of the measured and computed power spectral density of the velocity of the shell, computed up to 3000 Hz, it has been necessary to extrapolate (by a re-linear extrapolation) the value of the spanwise correlation length $L_\xi(f)$.

Originally, Corcos expressed the streamwise and spanwise coherences with the similarity variables $\omega\xi/U_c$ and $\omega\eta/U_c$ in an exponential form, given by

$$A(\xi, f) = \exp(-c_1|2\pi f\xi/U_c|), \quad B(\xi, f) = \exp(-c_2|2\pi f\omega\eta/U_c|), \quad (10, 11)$$

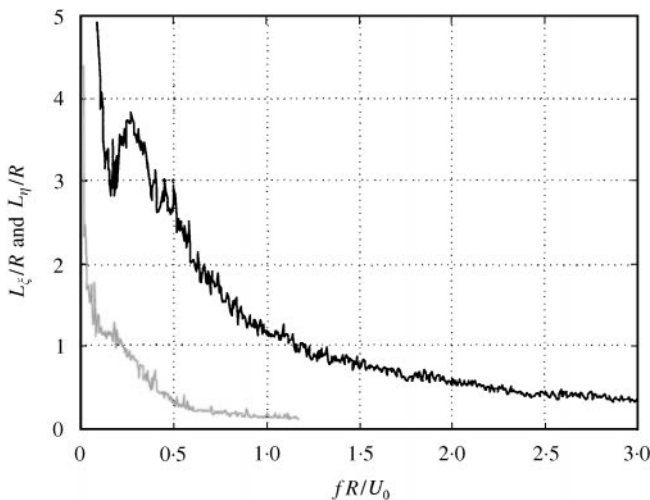


Figure 7. Streamwise (—) and spanwise (---) correlation lengths for 100 m/s.

where c_1 and c_2 are empirically determined constants. Assuming these relationships, a mean value of 0.15 was obtained for c_1 for $U_0 = 100$ m/s. Values of c_1 ranging from 0.10 to 0.19 are reported in the literature while some scatter appears for c_2 [35]. With regard to the numerical predictions of the dynamic response of the shell, the streamwise and spanwise coherence have been used as expressed by equations (8) and (9) and a direct reading of the value of $L_\xi(f)$ and $L_\eta(f)$ in Figure 7.

The convection velocity $U_c(\xi, f)$ was obtained from the phase function of the cross-spectrum by

$$U_c(\xi, f) = \frac{-2\pi f \xi}{\theta(\xi, f)}. \quad (12)$$

Figure 8 presents the variation of the ratio $U_c(\xi, f)/U_0$ as a function of frequency for fixed ξ . In the low-frequency range, the convection velocity changes rapidly with ξ/R ; this phenomenon can be again explained by the presence of the acoustic component. Beyond this zone, the three curves decrease slightly and continuously with frequency for all ξ/R . This decrease expresses the fact that the convection velocity of the large turbulent structures associated with the low frequencies is higher than the convection velocity associated with the small structures. The evolution of the ratio $U_c(\xi, f)/U_0$ with respect to ξ/R is characterized by an upward shift as ξ/R increase. Some investigators [26] have already pointed out this phenomenon. The spacing between microphones acts somewhat as a filter; the more it increases the more the contribution of smaller structures is filtered because they vanish more rapidly. At larger spacings, the convection velocity is thus governed by larger structures whose convection velocity is greater than that of smaller structures. That the ratio $U_c(\xi, f)/U_0$ was found to be between 0.7 and 0.8 is

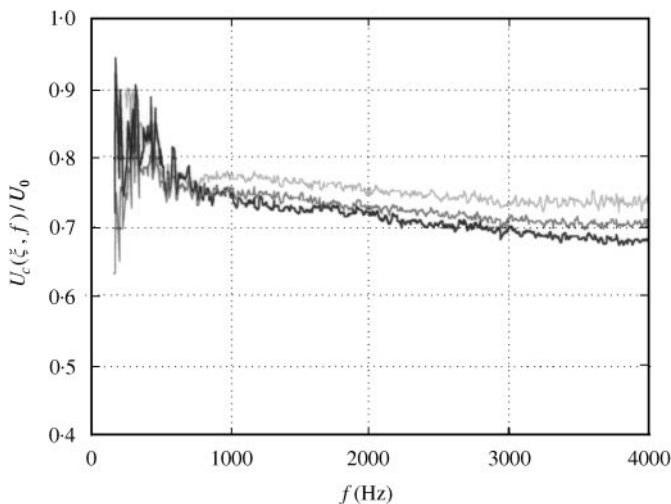


Figure 8. Measured ratio $U_c(\xi, f)/U_0$ as function of the frequency ($U_0 = 100$ m/s). ξ/R values: —, 0.128; —, 0.384; —, 0.784.

in good agreement with the literature. Some analytical expressions of the convection velocity have been proposed [35, 36]. In the paper by Graham [33], the influence of the convection velocity formulation has been studied. Here, no analytical identification of the convection speed has been attempted and the numerical predictions use directly the computed values of $U_c(\xi, f)$ presented in Figure 8.

3.4. MODEL OF THE CROSS-SPECTRUM

The spectral and cross-spectral features of the wall pressure fluctuations were analyzed in order to provide a model of the excitation usable for the numerical predictions. Thus, the cross-spectrum based on the model introduced by Corcos could be expressed by

$$\Phi_p(\xi, \eta, f) = \Phi_p^0(f) \exp\left(\frac{-|\xi|}{L_\xi(f)}\right) \exp\left(\frac{-|\eta|}{L_\eta(f)}\right) \exp\left(\frac{-i2\pi f \xi}{U_c(\xi, f)}\right), \quad (13)$$

where $\Phi_p^0(f)$, $L_\xi(f)$, $L_\eta(f)$ and $U_c(\xi, f)$ have been measured or computed over a wide range of frequency and for the four reference velocities 60, 80, 100 and 120 m/s. Our model differs from the Corcos one by the dependence of $L_\xi(f)$, $L_\eta(f)$ and $U_c(\xi, f)$ on the frequency. Therefore, a database characterizing the excitation produced by the fully developed turbulent pipe flow is now available. This database is completed by the measurements of the vibroacoustic response of the pipe test section. The accuracy of the excitation model and the numerical computation can now be appreciated by comparing the numerical predictions with the measurements of vibroacoustic response.

4. THEORETICAL MODEL

4.1. STATEMENT OF THE PROBLEM

Consider a thin elastic (or viscoelastic) cylindrical shell of finite length extended up to infinity by two rigid cylinders. Let Ω_i be the interior domain, formed by the interiors of the shell and the baffle, Ω_e the exterior domain, and Σ the domain occupied by the shell. In cylindrical co-ordinate (z, ϕ, r) , Σ occupies the domain $z \in]-L, +L[$, $\phi \in [0, 2\pi[$, $r = R$. The two semi-infinite baffles occupy the domains $\Sigma^-(z < -L)$ and $\Sigma^+(z > +L)$. $\bar{U} = (U_z, U_\phi, U_r)$ is the displacement vector of the shell, $P_{i,e}$ are the internal and external acoustic sound pressures radiated by the shell and \bar{F} is any representation of the turbulent wall pressure fluctuation. ρ_c is the density of the shell and $\rho_{i,e}$ the densities of the internal and external fluids.

An important point is that we neglect the influence of the internal flow in the wave propagation equation. As shown by Sgard and Atalla [37], for a Mach number less than roughly 0.5, there is a little influence of the mean flow velocity on the natural vibration characteristics of a plate in contact with air flow. Only a small

TABLE 1

Evolution of some measured resonance frequencies (Hz) with the Mach number

Mach 0	565	793	920	960	1131	...	1823
Mach 0.2	565	794	920	960	1132	...	1823
Mach 0.3	566	796	920	964	1134	...	1823
Mach 0.4	568	798	921	964	1136	...	1823

frequency shift of the spectrum of natural frequencies of the plate toward the low-frequency domain is observed. We have verified that this remains true for our configuration. To do this, a series of measurements of the spectrum of the shell response to an impact excitation hammer with and without flow was performed. The results are given in Table 1 in which some measured resonance frequencies are given for various Mach numbers. One can see that, for the Mach number used in this study ($M < 0.4$), the flow inside the shell has a little influence on the response of the shell. The only effect that can be noted is a small increase of the first five resonance frequencies, the others do not change (at least up to the 18th resonance frequency 1823 Hz). The flow inside the shell adds stiffness to the shell.

The corresponding acoustic pressure $P_{i,e}$ and the displacement of the shell $\bar{U}(M, t)$ are the solutions of the following system of partial differential equations:

$$\left[\Delta - \frac{1}{c_i^2} \frac{\partial^2}{\partial t^2} \right] P_i(M, t) = 0, \quad M \in \Omega_i, \tag{14}$$

$$\left[\Delta - \frac{1}{c_e^2} \frac{\partial^2}{\partial t^2} \right] P_e(M, t) = 0, \quad M \in \Omega_e, \tag{15}$$

$$\left[\bar{C} + \rho_c h \frac{\partial^2}{\partial t^2} \right] \bar{U}(Q, t) + \bar{P}(Q, t) = \bar{F}(Q, t), \quad Q \in \Sigma, \tag{16}$$

$$\frac{\text{Tr } \partial_r P_i(Q, t)}{\rho_i} = \frac{\text{Tr } \partial_r P_e(Q, t)}{\rho_e} = - \frac{\partial^2 U_r(Q, t)}{\partial t^2}, \quad Q \in \Sigma, \tag{17}$$

$$= 0, \quad Q \in \Sigma^- \cup \Sigma^+. \tag{18}$$

Here $\bar{P}(Q, t) = [0, 0, \text{Tr}(P_e - P_i)]$ is the pressure difference across the surface of the shell. The trace operator is defined as $\text{Tr } P_{e,i}(Q) = \lim_{M \rightarrow Q} P_{e,i}(M)$, $M \in \Omega_{e,i}$, $Q \in \Sigma$. The components of the excitation force $\bar{F}(Q, t)$ are $(0, 0, F(Q, t))$. Tr is the trace operator; for example $\text{Tr } \partial_r P_{i,e}(Q, t)$ is the value of the normal derivative of the acoustic sound pressure at the surface of the shell. \bar{C} is a thin shell operator. The first model adopted was the classical Donnell–Mushtari [38] operator but the first comparison reveals that this model may be not sufficient for a good description of the shell. The discrepancy between the experiment and the theory increases with the frequency. The ratio $h/R \simeq 1\%$ of the shell studied here seems to be a limit for the

Donnell–Mushtari operator [38]. We use one of the finest models of the thin shell operator, the Flügge operator [38, 39], which seems to give good results. To these equations, it is necessary to add boundary conditions for the displacement and a condition of conservation of the energy of the total system (outgoing wave condition for the acoustic pressure).

4.2. RESPONSE OF THE STRUCTURE TO THE TURBULENT EXCITATION

The turbulent wall pressure excitation is a space–time random process. Under some not very restrictive assumptions, such a process can be characterized by a cross-power spectral density $\Phi_p(Q; Q', \omega)$ where ω is the angular frequency. As seen in the previous section, $\Phi_p(Q; Q', \omega)$ is expressed in separable form. Let (z, ϕ) be the co-ordinates of Q and (z', ϕ') that of Q' ; $\Phi_p(Q; Q', \omega)$ is given by

$$\Phi_p(Q; Q', \omega) = \Phi_p(\xi, \eta, \omega), \quad (19)$$

where $\xi = z - z'$ and $\eta = \phi - \phi'$ are the axial (streamwise) and azimuth (spanwise) separations. The complete expression of this power spectral density is given in equation (13). Let $[\bar{u}(Q; M, \omega), p_i(Q; M, \omega), p_e(Q; M, \omega)]$ be the response of the system at M to a point unit harmonic normal force $(0, 0, \delta_Q)$ applied at Q . The cross-spectral densities of each component U_j of the displacement (U_z, U_ϕ, U_r) and of the acoustic sound pressure $P_{i,e}$ are given by

$$S_{U_j}(M; M', \omega) = \int_{\Sigma} \int_{\Sigma} u_j(Q; M, \omega) \Phi_p(Q; Q', \omega) u_j^*(Q'; M', \omega) dQ dQ', \quad (20)$$

$$S_{P_i}(M; M', \omega) = \int_{\Sigma} \int_{\Sigma} p_i(Q; M, \omega) \Phi_p(Q; Q', \omega) p_i^*(Q'; M', \omega) dQ dQ', \quad (21)$$

$$S_{P_e}(M; M', \omega) = \int_{\Sigma} \int_{\Sigma} p_e(Q; M, \omega) \Phi_p(Q; Q', \omega) p_e^*(Q'; M', \omega) dQ dQ', \quad (22)$$

where u_j , which is one of the three components u_z, u_ϕ, u_r and $p_{i,e}$ are the response of the shell to a normal point force. u_j^* and $p_{i,e}^*$ are the complex conjugate of u_j and $p_{i,e}$. The problem is reduced to solving a sequence of time harmonic problems. The main numerical difficulty is to obtain $\bar{u}, p_{i,e}$.

In the following, we consider only time harmonic problems with time dependency, hereafter omitted, $e^{-i\omega t}$.

4.3. GREEN'S REPRESENTATION OF THE PRESSURE

Let $k_{i,e} = \omega/c_{i,e}$ be the wave numbers in the internal and external fluids. Let $\mathcal{G}_\omega^{i,e}(M; M')$ be the Green functions of the interior and exterior Neumann problems

for the Helmholtz equation, defined as the solution of

$$\left[\Delta + k_{i,e}^2 \right] \mathcal{G}_\omega^{i,e}(M; M') = \delta_{M'}(M)M, M' \in \Omega_{e,i},$$

$$\partial_n \mathcal{G}_\omega^{i,e}(M; M') = 0 \text{ on } \Sigma^- \cup \Sigma \cup \Sigma^+, \quad \text{Sommerfeld radiation condition.}$$

One obtains for the acoustic pressure

$$p_{i,e}(M; M', \omega) = \omega^2 p_{i,e} \int_\Sigma u_r(Q; M', \omega) \mathcal{G}_\omega^{i,e}(M', Q) dQ, \quad (23)$$

where $\mathcal{G}_\omega^e(M; M')$ is given by the inverse Fourier transform with respect to the axial variable z of the function

$$\begin{aligned} \hat{\mathcal{G}}_\omega^e(r, \phi, \zeta; r', \phi', z') &= -\frac{i}{4} H_0(K_e d(M; M')) \\ &+ \frac{i}{4} \sum_{m=-\infty}^{+\infty} \frac{J'_m(K_e R) H_m(K_e r')}{H'_m(K_e R)} H_m(K_e r) e^{im(\phi - \phi')} e^{-2i\pi\zeta z'}, \end{aligned} \quad (24)$$

where $d(M, M')$ is the distance between the two points $M(z, \phi, r)$ and $M'(z', \phi', r')$. $H_m(x)$ is the Hankel function of the first kind of order m , and $H'_m(x)$ its derivative with respect to the argument. For simplicity, and because no confusion is possible between the two kinds of Hankel functions, the superscript (1) of the Hankel function of the first kind has been omitted. $J_m(x)$ is the Bessel function of the first kind of order m . $K_e^2 = k_e^2 - 4\pi^2\zeta^2$, $\Im K_e > 0$. $\mathcal{G}_\omega^i(M; M')$ is given by a series of normal modes [40],

$$\mathcal{G}_\omega^i(z, \phi, r; z', \phi', r') = \sum_{mn} \frac{\psi_{mn}(r, \phi) \psi_{mn}^*(r', \phi') e^{i\chi_{mn}|z - z'|}}{2i\chi_{mn}}, \quad (25)$$

where $\psi_{mn}(r, \phi) = A_{mn} J_m(\kappa_{mn} r) e^{im\phi}$ is the normal mode of order (mn) of the guide section. A_{mn} is a normalization factor, $\chi_{mn}^2 = k_i^2 - \kappa_{mn}^2$ with $\Im \chi_{mn} > 0$ if $\Im \chi_{mn} \neq 0$ and $\Re \chi_{mn} > 0$ if $\Im \chi_{mn} = 0$, $J'_m(j'_{m,n}) = 0$ and $\kappa_{mn} = j'_{m,n}/R$.

$\mathcal{G}_\omega^e(M; M')$ is defined for any real frequency. By its Green's representation, the external pressure is known as soon as the normal displacement of the shell is known. The Green's representation of the internal pressure is not defined for the cut-off frequencies of the waveguide, i.e., for $k_i = \kappa_{mn}$ [41].

4.4. TRANSFORMATION OF THE INITIAL PROBLEM INTO A BOUNDARY VALUE PROBLEM INSIDE A FINITE DOMAIN

In order to avoid this problem of non-existence of the solution, the initial problem is transformed into a boundary value problem inside a finite domain for

which the Green's representation of the pressure is defined for each frequency. Let σ^- be the cross-section of the cylinder located at $z = -L$ and σ^+ that located at $z = +L$. They define three domains $\Omega_i^-(z < -L)$, $\Omega_i^0(-L < z < L)$ and $\Omega_i^+(z > L)$. The corresponding acoustic pressures are denoted by $p_i^-(Q; M; \omega)$, $p_i^0(Q; M; \omega)$ and $p_i^+(Q; M; \omega)$. One has [41]

$$p_i^-(Q; M, \omega) = - \sum_{mn} \psi_{mn}(r, \phi) e^{-i\chi_{mn}(z+L)} \int_{\sigma^-} \psi_{mn}^*(r', \phi') p_i^0(Q; M', \omega) dM', \quad (26)$$

$$p_i^+(Q; M, \omega) = + \sum_{mn} \psi_{mn}(r, \phi) e^{+i\chi_{mn}(z-L)} \int_{\sigma^+} \psi_{mn}^*(r', \phi') p_i^0(Q; M', \omega) dM'. \quad (27)$$

These expressions are defined for any real frequency. Then the initial problem reduces to a boundary value problem inside a finite domain:

$$(\bar{C}_c - \rho_c h \omega^2) \bar{u}(Q; Q', \omega) - \begin{pmatrix} 0 \\ 0 \\ p_i^0(Q; Q', \omega) \end{pmatrix} = \begin{pmatrix} 0 \\ 0 \\ \delta_{Q'}(Q) \end{pmatrix}, \quad \begin{cases} Q = (z, \phi, R) \\ Q' = (z', \phi', R) \end{cases} \in \Sigma, \quad (28)$$

$$(\Delta + k_i^2) p_i^0(M; M', \omega) = 0, \quad \begin{cases} M = (z, \phi, r) \\ M' = (z', \phi', r') \end{cases} \in \Omega_i^0, \quad (29)$$

$$\partial_r p_i^0(Q; Q', \omega) = \rho_i \omega^2 u_r(Q; Q', \omega), \quad \begin{cases} Q = (z, \phi, R) \\ Q' = (z', \phi', R) \end{cases} \in \Sigma, \quad (30)$$

$$\partial_z p_i^0(Q; Q', \omega) = \pm \sum_{mn} \psi_{mn}(r, \phi) i\chi_{mn} \int_0^{2\pi} \int_0^R \psi_{mn}^*(r'', \phi'') p_i^0(Q''; Q', \omega) r'' dr'' d\phi'',$$

$$\begin{cases} Q = (\pm L, \phi, r) \\ Q' = (\pm L, \phi', r') \in \sigma^\pm, \\ Q'' = (\pm L, \phi'', r'') \end{cases} \quad (31)$$

where

$$\bar{C}_c \bar{u} = \bar{C} \bar{u} + \omega^2 \begin{pmatrix} 0 \\ 0 \\ \rho_e \int_\Sigma \mathcal{G}_\omega^e u_r \end{pmatrix} \quad (32)$$

is the shell operator which includes the external fluid loading. To this, it is necessary to add boundary conditions for $\bar{u}(Q; M; \omega)$. Equation (31) is a non-local boundary condition. The equations governing the coupling of the shell to an external fluid have a unique solution for any real frequency.

4.5. LIGHT FLUID APPROXIMATION AND MATCHED ASYMPTOTIC EXPANSION

In this section, to shorten the paper, we present only the method. The details of the analysis are given in Appendix A. When the density of the fluid is small compared to that of the shell, it is possible to build a solution of the problem by a perturbation method [42] which is powerful from a numerical point of view. Now let $\varepsilon = \rho_i/\rho_c h$ which is a small parameter for a steel thin shell in contact with air.

The method of matched asymptotic expansion is based on the remark that we can build two different expansions of the response of the shell (displacement or acoustic pressure inside the shell). The outer expansion which is valid far from the cut-off frequencies and the inner expansion which is valid at and near these frequencies. Besides, in this method, it is assumed that there exists an interval, named the overlap interval, around the cut-off frequencies in which the inner and outer expansions are both valid. These expansions are combined to construct a composite expansion valid everywhere.

4.5.1. Outer expansion

The solution is sought as a formal series in ε :

$$\bar{u}^o = \bar{U}^0 + \varepsilon \bar{U}^1 + \dots, \quad (p_i^o)^o = \Psi^0 + \varepsilon \Psi^1 + \dots \tag{33, 34}$$

It is to be noted that ε has the dimension of the inverse of a length. But, even if we use *non-dimensional* (or preferably *reduced*) equations its physical dimensions do not change. A length remains a length even if it is measured in a unit adapted to the problem. If we use a small non-dimensional parameter $\varepsilon_0 = \rho_i/\rho_c$, the formal series of \bar{u}^o reads

$$\bar{u}^o = \bar{W}^0 + \varepsilon_0 \bar{W}^1 + \varepsilon_0^2 \bar{W}^2 + \dots,$$

and it can be shown that $\bar{W}^0 = \bar{U}^0$, $\bar{W}^1 = \bar{U}^1/h$, \dots , $\bar{W}^n = \bar{U}^n/h^n$, and the two series are identical; we have chosen the small parameter ε which appears to be most significant for the fluid loading of thin structure. Let $\bar{\Gamma}_\omega$ be the Green operator of the finite shell loaded by the external fluid (defined for each frequency). Only a numerical solution of it is known. It is easy to show that the zeroth order approximation is given by

$$\Psi^0 = 0, \quad \bar{U}^0 = \bar{\Gamma}_\omega(\bar{e}_r \delta_Q), \tag{35, 36}$$

where \bar{e}_r is the unit vector normal to the shell. In the same way, the first order approximation is given by

$$\Psi^1 = -\rho_c h \omega^2 \sum_{mn} \psi_{mn}(r, \phi) \int_\Sigma U_r^0 \psi_{mn}^*(r', \phi') \frac{e^{i\chi_{mn}|z-z'|}}{2i\chi_{mn}}, \quad \bar{U}^1 = \bar{\Gamma}_\omega(\bar{e}_r \Psi^1). \tag{37, 38}$$

As previously stated, this solution is not defined at the cut-off frequencies of the internal waveguide. It is then necessary to seek another approximation [6], which is defined close to and at these frequencies (the inner expansion).

4.5.2 Inner expansion

Close to the angular frequency $\omega_{pq} = c\kappa_{pq}$, one can define $\omega = \omega_{pq}(1 + \varepsilon^2\alpha)$. The solution is sought again as a power series in ε :

$$\bar{u}^i = \bar{V}^0 + \varepsilon\bar{V}^1 + \dots, \quad (p_i^0)^i = \bar{\Psi}^0 + \varepsilon\bar{\Psi}^1 + \dots \tag{39, 40}$$

Then

$$\chi_{mn} \neq 0 \quad \forall \varepsilon \text{ and } (m, n) \neq (p, q), \quad \chi_{pq} \simeq \kappa_{pq} \left[1 + \frac{\alpha\varepsilon^2}{4} + \dots \right] \varepsilon\sqrt{2\alpha}. \tag{41, 42}$$

One shows that the zeroth order approximation depends on an undetermined constant A_{pq} :

$$\bar{\Psi}^0 = A_{pq}\psi_{pq}, \quad V^0 = \bar{\Gamma}_\omega[\bar{e}_r\delta_Q + \bar{e}_rA_{pq}\psi_{pq}]. \tag{43, 44}$$

To evaluate it, one can write the equation satisfied by $\bar{\Psi}^1$ which is a homogeneous equation with non-homogeneous boundary conditions on Σ . A solution exists if and only if the data satisfy a compatibility condition which leads to the value of A_{pq} :

$$A_{pq} = - \frac{\omega_{pq}^2 \rho_c h \int_\Sigma (\bar{\Gamma}_\omega(\bar{e}_r \delta_Q(Q)))_r \psi_{pq}(Q)^* dQ}{2i\kappa_{pq} \sqrt{2\alpha} + \omega_{pq}^2 \rho_c h \int_\Sigma (\bar{\Gamma}_\omega(\bar{e}_r \psi_{pq}(Q)))_r \psi_{pq}^*(Q) dQ}. \tag{45}$$

The next step is to show that the validity domains of the inner and outer expansions overlap on a small domain around the cut-off frequency ω_{pq} . To do this, it is necessary to verify that the matching principle is satisfied [5]. That is $(\bar{u}^i)^o = (\bar{u}^o)^i$, or, in other words, the outer expansion of the inner expansion is equal to the inner expansion of the outer expansion. Then, the composite expansion, regular for each frequency, is given by

$$\bar{u} = \bar{u}^o + \bar{u}^i - (\bar{u}^i)^o. \tag{46}$$

Practically, the outer expansion and the exact solution give quite identical results away from the cut-off frequencies. It seems preferable to use the numerical solution of the exact equations outside of these frequency domains. On the other hand, the inner expansion is necessary around these frequencies.

4.6. BOUNDARY INTEGRAL EQUATION METHOD TO SOLVE THE DETERMINISTIC HARMONIC BOUNDARY VALUE PROBLEM

The method developed in this section is valid for any frequency but the cut-off frequencies of the interior waveguide.

Owing to the 2π -periodicity of the geometry, each quantity is developed into a Fourier series with respect to the angular variable ϕ . One has

$$\bar{u}(z, \phi) = \sum_{m=-\infty}^{\infty} \bar{u}_m(z) e^{im\phi}, \quad p_{i,e}(z, \phi, r) = \sum_{m=-\infty}^{\infty} p_{mi,e}(z, r) e^{im\phi}, \quad (47, 48)$$

$$\bar{F}(z, \phi) = \sum_{m=-\infty}^{\infty} \bar{F}_m(z) e^{im\phi}. \quad (49)$$

For each angular harmonic, the equations of the problem are

$$\bar{C}_m \bar{u}_m(z) - \omega^2 \rho_c h \bar{u}_m(z) = \bar{F}_m(z) - \bar{p}_m(z) \quad \text{on } \Sigma, \quad (50)$$

$$(\Delta + k_{i,e}^2) p_{mi,e}(z, r) = 0 \quad \text{in } \Omega_{i,e}, \quad (51)$$

$$\text{Tr } \partial_{\bar{n}} p_{mi,e}(z, R) = \omega^2 \rho_{i,e} u_{rm}(z) \quad \text{on } \Sigma, \quad (52)$$

$$\bar{p}_m(z) = (0, 0, \text{Tr } p_{mi}(z, R) - \text{Tr } p_{me}(z, R)), \quad (53)$$

$$u_{zm}(\pm L) = u_{\phi m}(\pm L) = u_{rm}(\pm L) = u'_{rm}(\pm L) = 0, \quad (54)$$

$$\text{Sommerfeld condition for } p_{mi,e}(z, r), \quad (55)$$

where \bar{C}_m is the angular harmonic m of the thin shell operator and $u'_{rm}(z)$ is the derivative with respect to z of $u_{rm}(z)$. This problem is solved by using a boundary integral equation method [43]. The main difficulty of this method is that it requires the knowledge of the Green functions of the various operators involved.

4.6.1. Boundary integral equation method

As previously seen, the acoustic sound pressures are expressed in terms of the normal displacement of the shell. One has

$$\text{Tr } p_{mi,e}(z, R) = \pm \omega^2 \rho_{i,e} R \int_{-L}^L u_{rm}(z') G_{m\omega}^{i,e}(z - z') dz'. \quad (56)$$

The kernels denoted by $G_{m\omega}^{i,e}(z)$ are given by

$$G_{m\omega}^e(z) = \int_{-\infty}^{\infty} \frac{H_m(K_e R)}{K_e R H'_m(K_e R)} e^{2i\pi z \zeta} d\zeta, \quad G_{m\omega}^i(z) = \frac{1}{R^2} \sum_{n=0}^{\infty} \frac{\Psi_{mn} \Psi_{mn}^*}{\Lambda_{mn} \chi_{mn}} e^{i\chi_{mn}|z|}, \quad (57, 58)$$

where $K_e^2 - k_e^2 - 4\pi^2 \zeta^2$ with $\Im K_e > 0$, $\chi_{mn}^2 = k_i^2 - \kappa_{mn}^2$ and $\Psi_{mn} = \Lambda_{mn} J_m(\kappa_{mn} R)$, Λ_{mn} is a normalization factor.

One can now introduce the Green tensor of the *in vacuo* thin shell operator $\bar{\bar{I}}_m$ defined by

$$(\bar{\bar{C}}_m - \omega^2 \rho_c h \bar{\bar{I}}) \bar{\bar{I}}_m = \delta \bar{\bar{I}}, \tag{59}$$

where δ is the Dirac measure and $\bar{\bar{I}}$ is the identity matrix. This tensor is calculated without any difficulty by the residue integration theorem. $\bar{\bar{I}}_m$ is a 3×3 symmetrical matrix and each of its components is given by a linear combination of four complex exponential functions [43].

The solution of the problem is then given by the integral equations.

$$\bar{u}_m(z) = \bar{\bar{I}}_m(\bar{F}_m - \bar{p}_m + \bar{S}_m)(z), \tag{60}$$

$$\bar{p}_m(z) = (0, 0, \omega^2 R \int_{-L}^L u_{rm}(z') (\rho_e G_{m\omega}^e(z - z') + \rho_i G_{m\omega}^i(z - z')) dz'), \tag{61}$$

where

$$\bar{\bar{I}}_m(\bar{F}_m)(z) = \int_{-\infty}^{\infty} \bar{\bar{I}}_m(z - z') \bar{F}_m(z') dz', \quad \bar{\bar{I}}_m(\bar{p}_m)(z) = \int_{-L}^L \bar{\bar{I}}_m(z - z') \bar{p}_m(z') dz', \tag{62, 63}$$

$$\bar{\bar{I}}_m(\bar{S}_m)(z) = (\Gamma_{zm}^r(z \mp L) s_{1m}^{\pm L}, \Gamma_{\phi m}^r(z \mp L) s_{2m}^{\pm L}, \Gamma_{rm}^r(z \mp L) s_{3m}^{\pm L} + \Gamma_{rm}^r(z \mp l) s_{4m}^{\pm L}). \tag{64}$$

The boundary sources \bar{S}_m (which are scalars) have been introduced to take into account the boundary conditions at the edges of the shell. These sources introduce eight unknowns ($s_{im}^{\pm L}, i = 1, \dots, 4$) calculated by applying the boundary conditions for the displacement.

4.6.2. Numerical solution of the boundary integral equations

We have chosen the simplest numerical method, the collocation method [44], to solve these equations. The unknowns are sought as a linear combination of simple known functions (like piecewise constant functions, spline functions or orthogonal polynomial) $\beta(z), \gamma(z)$,

$$\bar{u}_m(z) = \sum_{j=1}^M \bar{u}_m^j \beta_j(z), \quad p_m(z) = \sum_{j=1}^N p_m^j \gamma_j(z),$$

and the integrals are satisfied at a finite number of points (the collocation points). Compared with the Galerkin method for which the distance between the solution and its approximation is minimized with respect to a norm, there is less computational effort (we need only the computation of one-dimensional integrals). Moreover, we have chosen the simplest approximation functions, i.e. piecewise constant functions. The number of collocation points is taken as equal to the number of unknowns (the coefficients of the linear combinations \bar{u}_m^j and p_m^j). The

precision of the method is achieved by increasing the number of collocation points M and N . In the general case, it is classical that a minimum of six points per wavelength is necessary to achieve a good precision (less than 1 dB). The main difficulty is a *a priori* knowledge of this wavelength which depends not only on the mechanical properties of the shell but also on its geometrical characteristics (such as length) and of the fluid loading. Obviously, close to a resonance frequency of the shell, it is necessary to refine the discretization (up to a 20th of the wavelength). For our problem, both fluids have a little influence on the shell, except close to the resonance frequencies, and then a rough approximation (two or three points per wavelength) of the pressure is sufficient.

After discretization, one obtains a linear system of $3M + N + 8$ simultaneous equations: $\bar{A}_m \bar{X}_m = \bar{B}_m$, in which \bar{A}_m is an almost full matrix. The coefficients of it depend analytically on the frequency ω . Except close to the cut-off frequencies, this system is solved without difficulty by using a LU decomposition. By anticipating the results, one can remark that in the Green representation of the pressure, the integral between the normal displacement and the Green functions is multiplied by ω^2 and while the density of the fluid is small, at high frequency the singularity of $G_{m\omega}^i(z)$ close to the cut-off frequencies introduces numerical instabilities (some extra diagonal terms are very important) and leads to very bad conditioning of the linear system.

5. NUMERICAL RESULTS AND COMMENTS

The mechanical characteristics of the shell are: length = 46 cm, radius = 6.25 cm, thickness = 0.5 mm, Young's modulus, $E_0 = 215$ GPa, the Poisson ratio, $\nu = 0.32$, density, $\rho_c = 7850$ kg/m³. Because the measurements reveal that the shell has a small damping, it has been introduced as a simplified viscous damping in the form of a complex Young's modulus $E = E_0(1 - i\zeta)$, $\zeta > 0$. The negative sign comes from the time dependency $\exp(-i\omega t)$ to ensure a finite value when the time increase. With a time dependency $\exp(+i\omega t)$, the complex Young's modulus has to be written $E = E_0(1 + i\zeta)$. The value $\zeta = 5 \times 10^{-4}$ was estimated from the measurements. The fluids are air with density $\rho_{i,e} = 1.3$ kg/m³ and sound speed $c_{i,e} = 340$ m/s.

5.1. CUT-OFF FREQUENCIES AND MATCHED ASYMPTOTIC EXPANSIONS

In Table 2, one can find the firsts (less than 10 kHz) cut-off frequencies (more precisely, their integer part) of the waveguide.

In our problem, the response of the shell is estimated to be below 3200 Hz, and so as can be seen, only a few cut-off frequencies may cause problems for the computations corresponding to the experiment analyzed here. In Figures 9–14 we present the results of the matched asymptotic expansion around (Figures 9, 11, and 13) and close to (Figures 10, 12 and 14) three cut-off frequencies: f_i^{11} , f_i^{21} and f_i^{31} . These frequencies are indicated in the figures by a vertical line. Obviously at these frequencies, the displacement, calculated by solving the boundary integral

TABLE 2
Cut-off frequencies (Hz) of the waveguide

f_i^{mn}	$n = 1$	$n = 2$	$n = 3$	$n = 4$
$m = 0$	0	3318	6074	8808
$m = 1$	1594	4616	7391	—
$m = 2$	2644	5806	8632	—
$m = 3$	3637	6940	9823	—
$m = 4$	4604	8037	—	—
$m = 5$	5557	9108	—	—

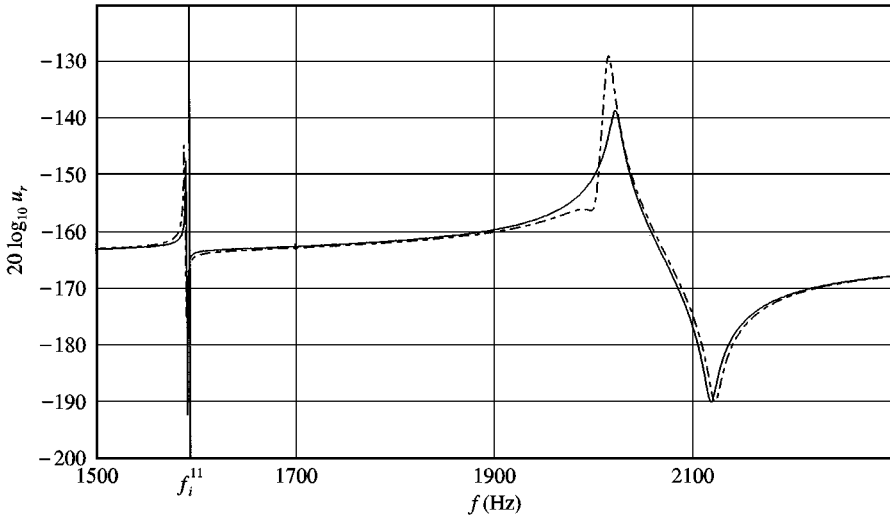


Figure 9. Comparison of the exact (—) and composite (---) expansion solutions: $m = 1$.

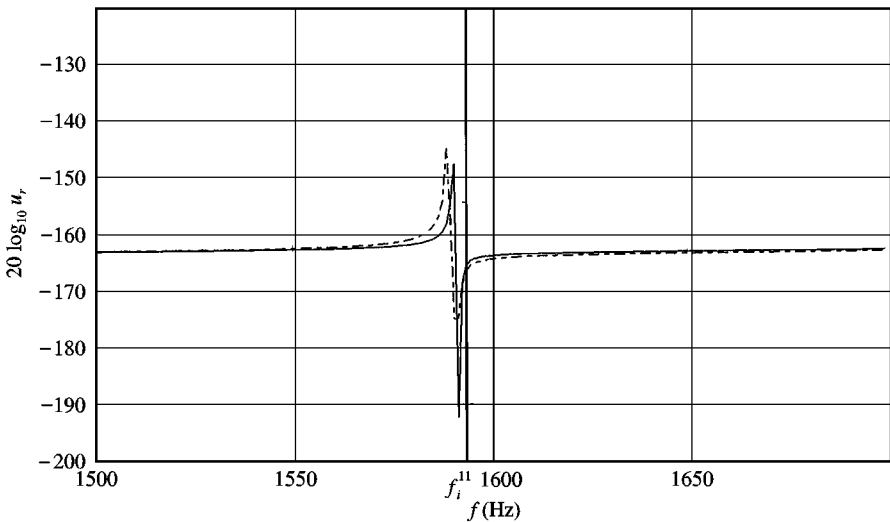


Figure 10. Enlargement of Figure 9 around f_i^{11} .

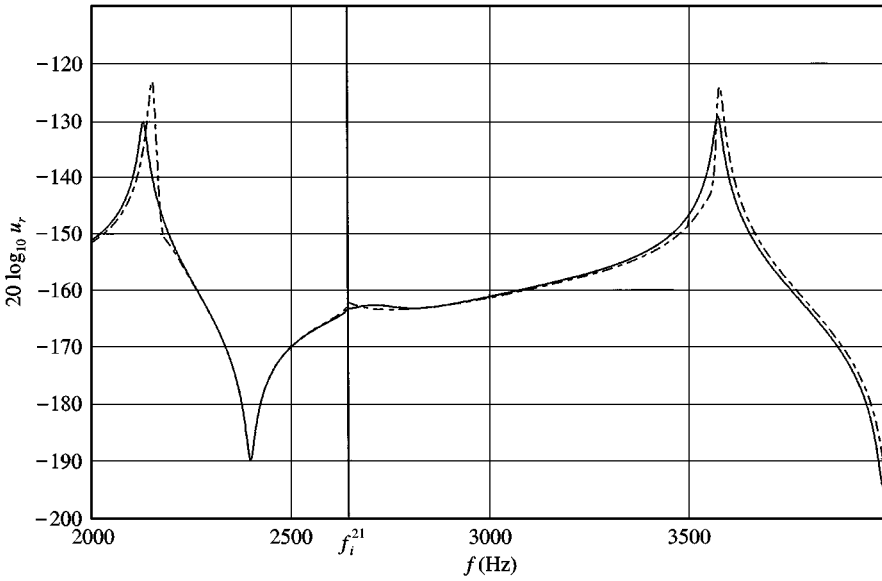


Figure 11. Comparison of the exact (—) and composite (---) expansion solutions: $m = 2$.

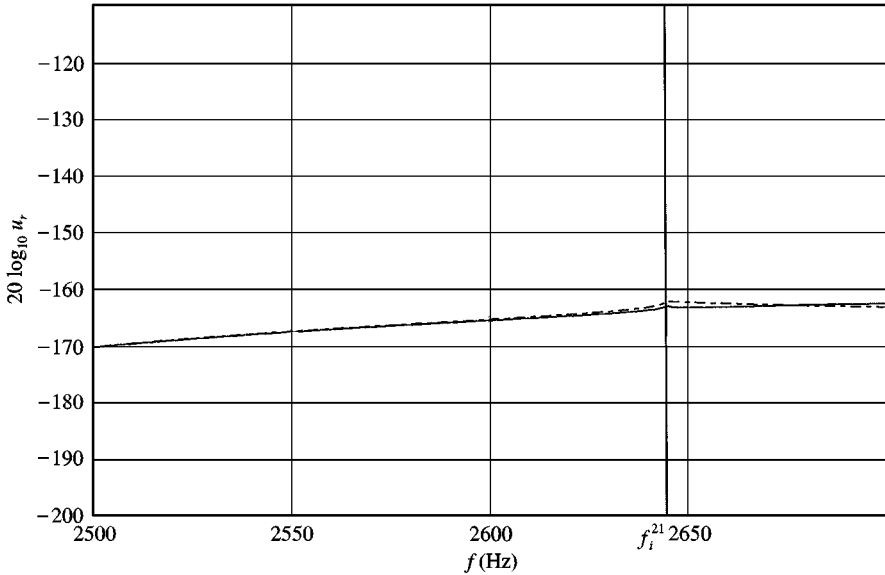


Figure 12. Enlargement of Figure 11 around f_i^{21} .

equations, is not defined. All the curves show the normal displacement of the shell u_{3m} at the excitation point $+L/\sqrt{2}$ with $m = 1$ (Figures 9 and 10), $m = 2$ (Figures 11 and 12) and $m = 3$ (Figures 13 and 14). The continuous curve represents the displacement solution of the boundary integral equations developed in the previous section, while the discontinuous curve is the result of the composite expansion. For the various angular harmonics, the composite expansion gives very good results

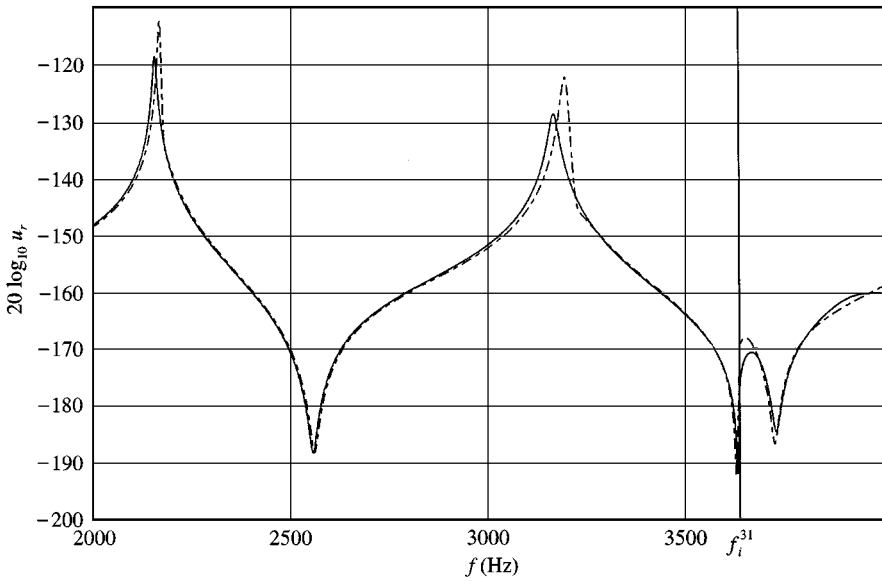


Figure 13. Comparison of the exact (—) and composite (---) expansion solutions: $m = 3$.

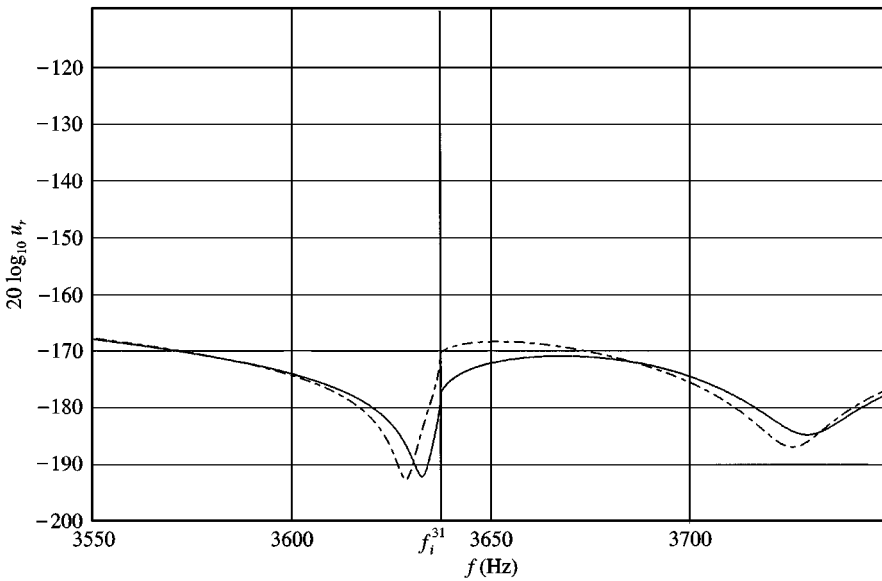


Figure 14. Enlargement of Figure 13 around f_i^{31} .

except close to the resonance frequencies of the shell. Nevertheless, close to the cut-off frequencies, where the solution of the boundary integral equations becomes infinite, the composite expansion gives very precise results. The Green representation of the pressure is singular only very close to the cut-off frequencies because the zeros of the Bessel functions are computed [45] by using 12 significant digits and the singularity of the denominator is proportional to $\sqrt{f - f_i^{mn}}$. The zero

of it is known with at least six digits. Close to some resonance frequencies of the fluid-loaded shell, the results of the composite expansion are deteriorating. The main difference between the exact and approximate solutions is the amplitude of the shell response. This is due to the outer expansion in which taking only two terms does not give sufficiently precise results. The internal fluid acts on the shell as a smaller order effect (the internal pressure is of order ε , see equations (36) and (38)) and then, close to the resonance frequencies of the shell where it has a strong influence, it is necessary to use more terms in the outer expansion to describe correctly the influence of the internal fluid. Nevertheless with a first order expansion, the damping, introduced both by the material damping and by fluid-loading effects (energy lost at infinity), is not modified (the relative bandwidth is preserved).

5.2. RESONANCE FREQUENCIES OF THE SHELL

5.2.1. Modal identification

We present here visualizations of the spectral density velocity of the shell, excited by the turbulent internal flow (for 100 m/s), close to three resonance frequencies. Measurements were obtained by a laser beam situated roughly at 2 m in front of the shell as it can be seen on the photograph of Figure 15. The welding joint is exactly in front of the beam. The image was obtained by using 32 points on the half circumference and 8 points along the generating axis. Because the laser beam can only do radial measurements, the values obtained close to the upper and lower

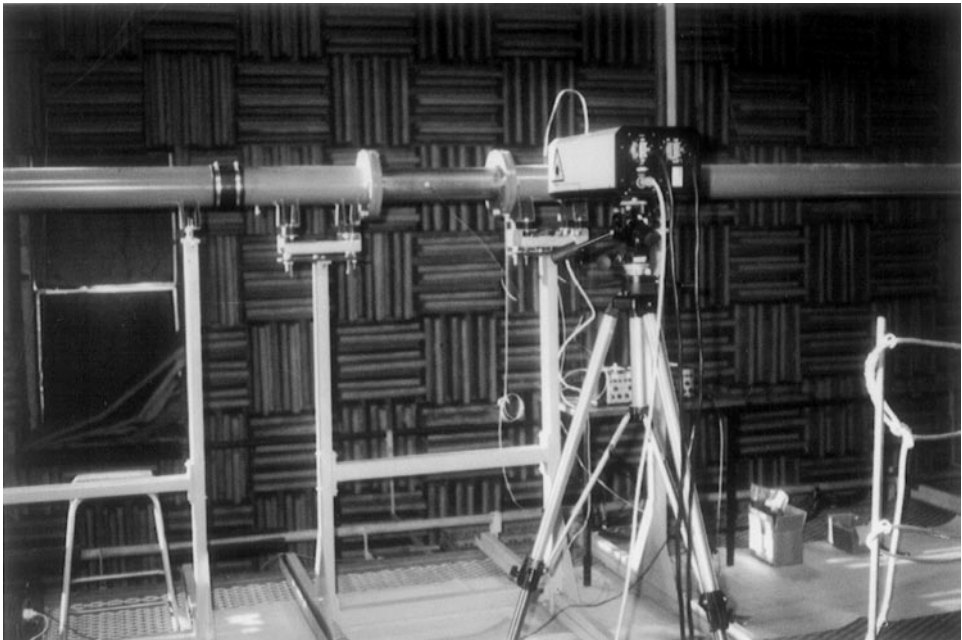


Figure 15. Laser measurements.

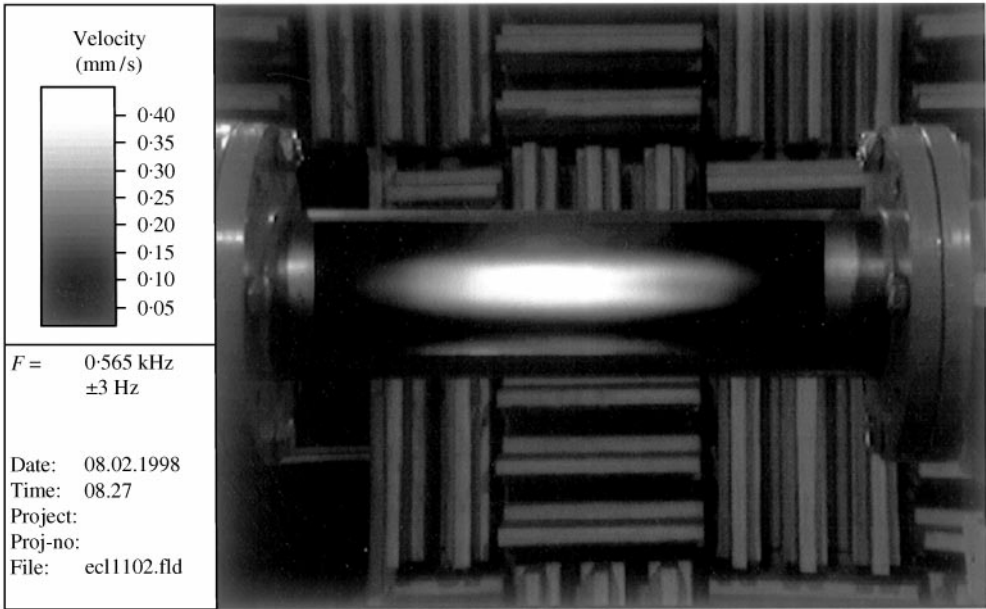


Figure 16. Mode 3, 1.

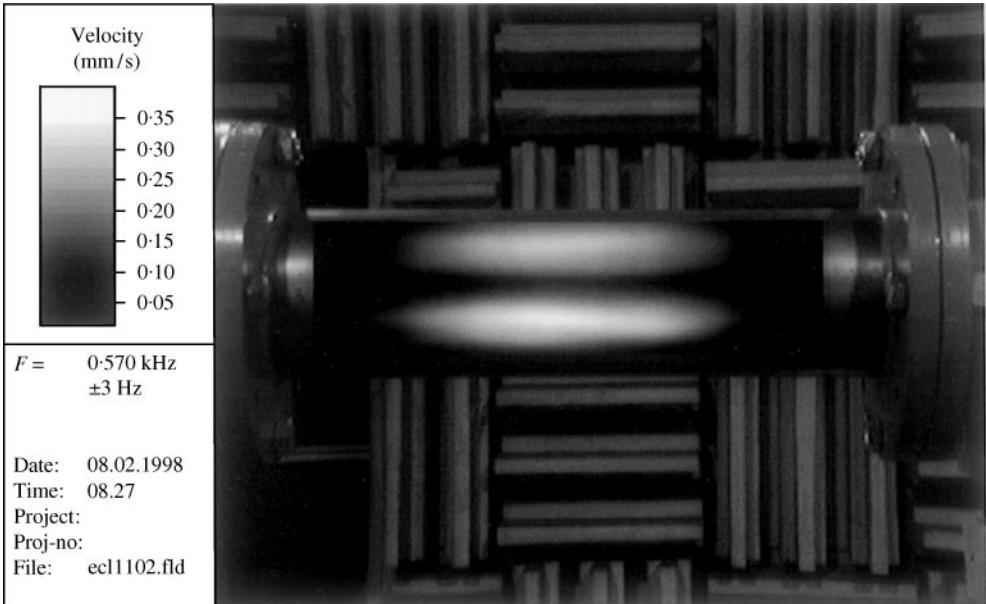


Figure 17. Mode 4, 1.

parts of the visualization plane are biased. Figure 16 presents the spectral density of the velocity for the mode (3, 1), Figure 17 that for the mode (4, 1) and Figure 18 that for the mode (5, 3). For all the modes presented here, the odd harmonic modes (i.e., the odd values of m) of the angular Fourier series have a minimum value on the

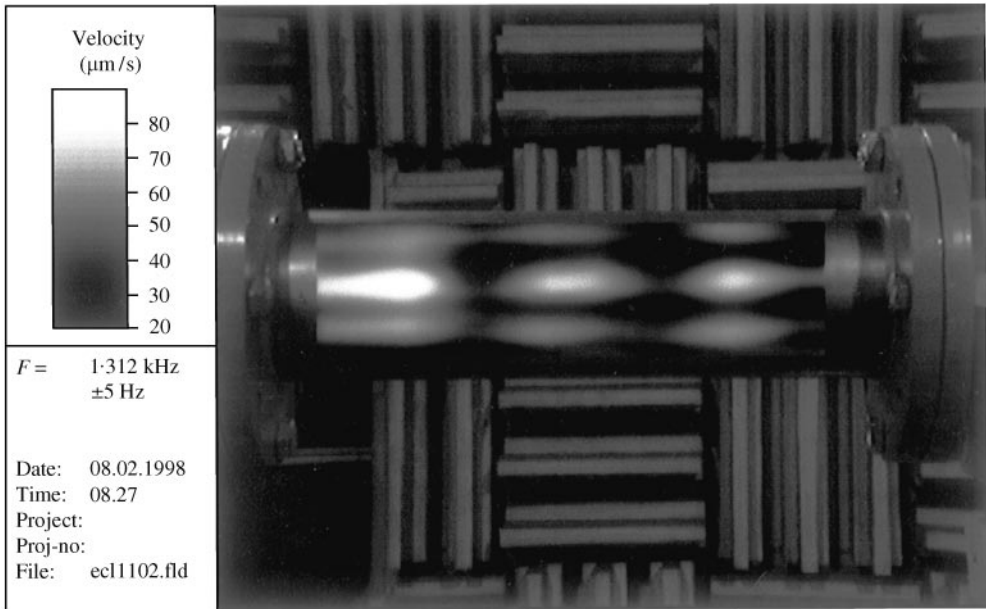


Figure 18. Mode 5, 3.

welding joint while the even harmonic modes have a maximum on it. The welding joint introduces a “singularity” that “defines” in some way the angular origin. It is to be noted that we have not observed modes doubled (as can appear for not exactly cylindrical shell). The shell used in this experiment is a quite perfect cylindrical shell.

5.2.2. Comparison between the measured and computed resonance frequencies

In Table 3 we present the first resonance frequencies of the fluid-loaded shell. These frequencies, which are the ones for which free oscillations are possible, are the frequencies that cancel the determinant of the matrix $\bar{A}_m(\omega)$ which analytically depends on the frequency. Let us briefly recall that the oscillations which correspond to the resonance modes are different (for frequency-dependent boundary condition) from the eigenmodes [40]. These frequencies are real for an elastic shell *in vacuo* and are calculated by looking for the real zero of the determinant of an 8×8 matrix of complex exponentials which is done very quickly. When the shell is slightly damped (by viscous damping or by fluid loading), its resonance frequencies are close to the real ones. Then, the complex resonance frequencies are calculated by using a simple Newton routine that converges very quickly (a few iterations) with the real frequencies as starters. In Table 3, the relevant first resonance frequencies for our problem are given. The *in vacuo* resonance frequencies have also been indicated (second lines for each harmonic) as italic and the measured (with an impact hammer) resonance frequencies as bold (third lines for some harmonics). It is to be noted that while we give only the frequencies for the seven first harmonics, it has been necessary for a complete model of the shell of the experiment to treat the 10 first harmonics.

TABLE 3

First resonance frequencies (Hz) of the shell: *f.l.*, fluid-loaded shell; *i.v.*, in vacuo shell; *m*, measurement

f_{mn}	$n = 1$	$n = 2$	$n = 3$	$n = 4$	$n = 5$	$n = 6$
$m = 1$ f.l.	(2105, -4.9)	(4249, -1)				
<i>i.v.</i>	(2095, -0.4)	(4241, -5.4)				
$m = 2$ f.l.	(972, -1.6)	(2223, -8.8)	(3730, -9)			
<i>i.v.</i>	(982, -0.7)	(2247, -1)	(3723, -1.3)			
<i>m</i>	919	—	—			
$m = 3$ f.l.	(574, -0.7)	(1305, -1.3)	(2255, -6.2)	(3306, -12.5)		
<i>i.v.</i>	(577, -0.7)	(1314, -1.1)	(2273, -1.4)	(3336, -1.5)		
<i>m</i>	565	1301	—	—		
$m = 4$ f.l.	(570, -0.5)	(944, -1.1)	(1552, -1.5)	(2293, -2.1)		
<i>i.v.</i>	(572, -0.5)	(948, -1)	(1559, -1.5)	(2306, -1.7)		
<i>m</i>	571	945	1560	—		
$m = 5$ f.l.	(795, -0.4)	(957, -0.9)	(1300, -1.4)	(1794, -1.8)	(2387, -2)	
<i>i.v.</i>	(797, -0.4)	(960, -0.8)	(1305, -1.4)	(1801, -1.8)	(2397, -2)	
<i>m</i>	795	960	1311	1815	—	
$m = 6$ f.l.	(1134, -0.4)	(1208, -0.7)	(1385, -1.2)	(1683, -1.6)	(2085, -2)	(2566, -2.2)
<i>i.v.</i>	(1137, -0.4)	(1212, -0.7)	(1390, -1.1)	(1688, -1.6)	(2092, -1.9)	(2574, -2.2)
<i>m</i>	1131	1206	1387	1700	—	—
$m = 7$ f.l.	(1550, -0.4)	(1592, -0.8)	(1690, -1)	(1863, -1.4)	(2120, -1.8)	(2453, -2)
<i>i.v.</i>	(1554, -0.3)	(1597, -0.6)	(1694, -0.9)	(1868, -1.3)	(2125, -1.7)	(2460, -2)
<i>m</i>	1544	1589	1689	1874	—	—

These results call for a few comments. First of all, as revealed by the very small imaginary part of the resonance frequencies, the shell is quite undamped and “rings like a bell”. Secondly, the frequency shift induced by the presence of the fluids cannot be reduced to only the usual added mass effect (which decreases the real part of the resonance frequencies). While the majority of the real parts of the resonance frequency decrease with the fluids, some have real parts that increase (see e.g., f_{11} , f_{23}); this effect is caused by the internal fluid which act as a spring (when the internal fluid is not taken into account, the resonance frequency f_{11} is given by 2093 - i4.9, and f_{23} is given by 3721 - i9). Another important point is that the fluid loading has a little influence on the shell. For most of the resonance frequencies, there is no dissipation introduced by the fluid; the imaginary part of the damped *in vacuo* and fluid-loaded resonance frequencies are identical (to the precision of the numerical method). For these frequencies, the response of the shell is strongly dependent on viscous damping. Only a few resonance frequencies present a significant increase of their imaginary part when the fluid is taken into account (see, e.g., f_{11} , f_{21} , f_{22} , f_{32} , f_{33} , f_{44} , ...). Then, only the resonance modes corresponding to these frequencies are affected by the presence of the fluid and then radiate into it. The shell does not radiate well at low frequencies.

The comparison with experimental results is very good (if one excepts f_{21} , the relative error is less than 2%) and correspond to the precision at which the mechanical parameters of the shell (built with industrial material) are known.

6. COMPARISON OF THE MEASURED AND COMPUTED VIBROACOUSTIC RESPONSE OF THE SHELL

6.1. VELOCITY OF THE SHELL

In this section, we present a comparison, given in Figure 19, between the measured and calculated power spectral densities of the velocity of a point on the shell $S_{v_r} = -\omega^2 S_{u_r}$, where S_{u_r} is given by equation (20). The measurement point is located at 20 cm upstream of the extremity of the shell. The velocity at the center of the pipe is 100 m/s.

Again, the results are very good. The results are sufficiently precise for the acoustician. Except at low frequency where the measurements seem noisy and very close to some resonances of the shell, where the amplitude is very sensitive to the damping of the experimental set-up, the two curves are in good agreement within the accuracy of the measure which has about 50 dB dynamic range. With a third-octave analysis, the discrepancy between the experiment and the theory is about 2 dB (see Figure 20). It must be noted that due to the limited measurement dynamic range, the minimal levels of the shell response are overestimated. The models of the fluid-loaded shell and of the turbulent pressure fluctuations are very precise. Ten angular harmonics have been taken into account. The frequency step is 1 Hz. It is to be noted that the computation is very fast: less than 1 h on a 400 MHz PC. Because the fluid has a small influence on the shell, one can compute the

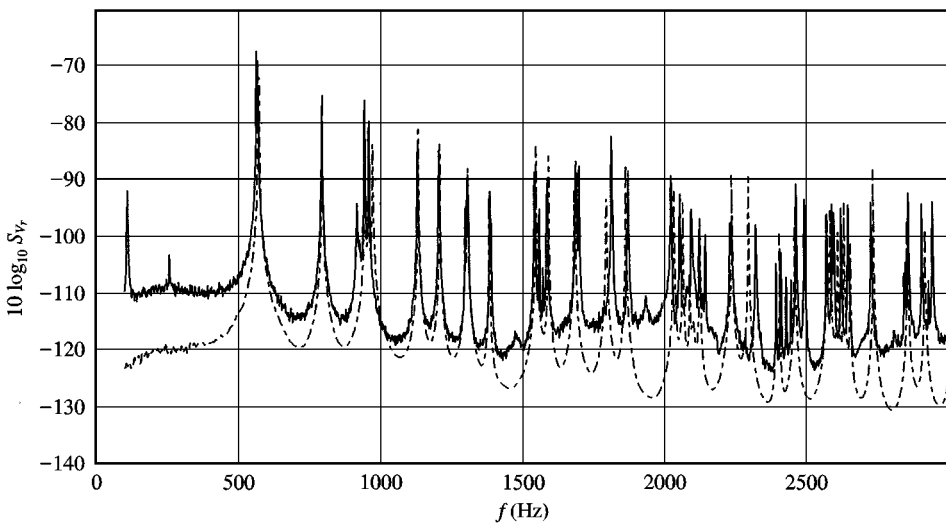


Figure 19. Power spectral density of the velocity of the pipe, ---, model; —, measurement.

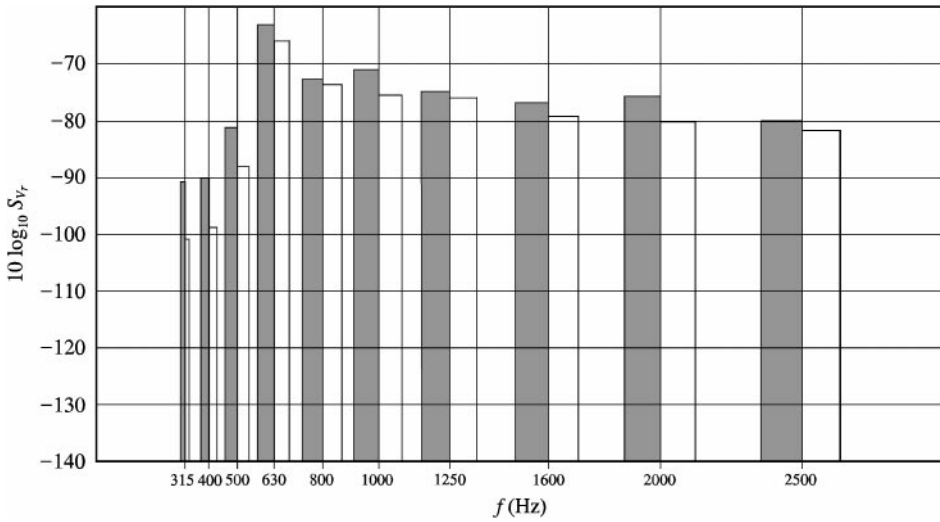


Figure 20. Comparison between the measured (■) and computed (□) mean (third-octaves) power spectral densities of the velocity of the pipe.

dynamic response for the shell *in vacuo* excited by the turbulent wall pressure fluctuations with a fairly good agreement. But some of the resonance frequencies are shifted up to 20 Hz and their amplitudes show an increase of about 20 dB. Moreover, the boundary element method is so efficient that the computation times for the evaluation of the response of the fluid-loaded and *in vacuo* shells are quite identical.

6.2. ACOUSTIC PRESSURE RADIATED BY THE SHELL

The last results, given in Figure 21, show a comparison between computed and measured power spectral density of the pressure outside the shell S_{P_e} given by equation (22). Figure 22 presents the results with a third-octave analysis. The microphone is situated at 10 cm upstream of the extremity of the shell at a radial distance of 5 mm. Such a small distance from the shell was necessary because, as it has been seen, the shell does not radiate well at these frequencies. Except at low frequency, the measurements are not very good. Even if the two curves look similar, the amplitude of the resonance modes is always underestimated and leads to a bad third-octave analysis at high frequency. Another limitation of the comparison lies in the fact that above 1800 Hz the sound radiation by the pipe conveying the air flow has a level comparable to that of the test section. The shaded zone that appears in Figure 21 is a frequency range where the comparison between theory and experiment is not significant.

At 20 cm from the shell the frequency measurements are very difficult below 3000 Hz because only a small number of modes contribute to the radiation of the shell (roughly four or five). Only four or five peaks emerge from the background noise. However, from a theoretical point of view, it is not very important that the

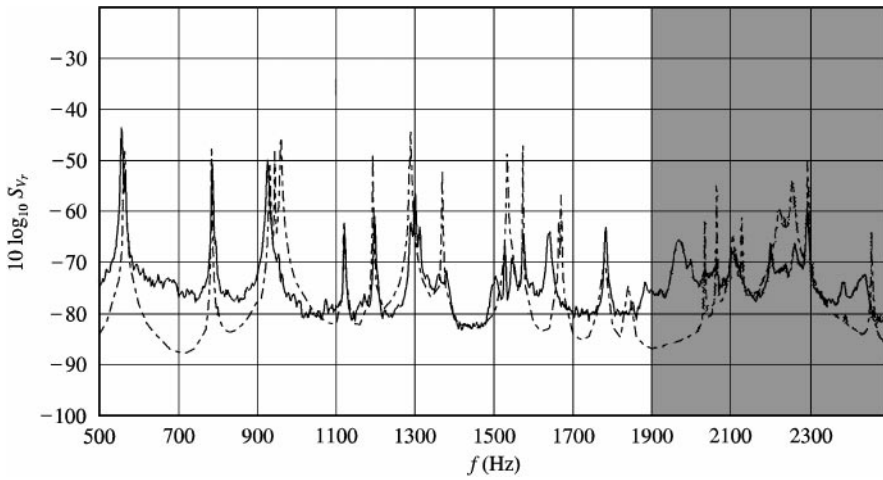


Figure 21. Power spectral density of the pressure radiated by the pipe. ---, model; —, measurement.

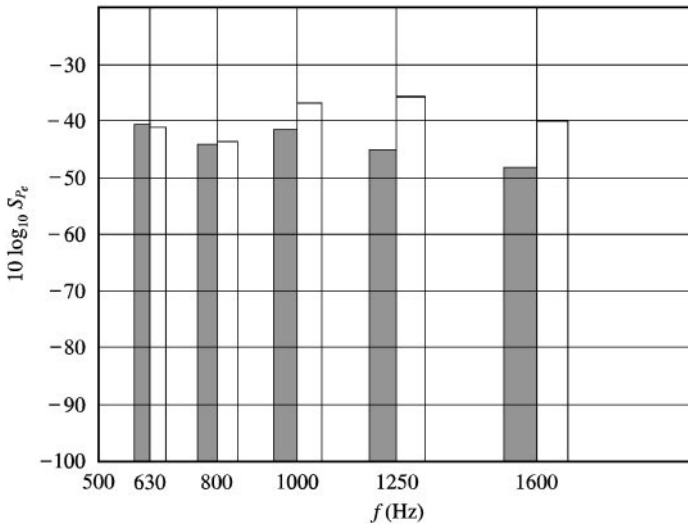


Figure 22. Comparison between the measured (■) and computed (□) mean (third-octaves) power spectral densities of the pressure radiated by the pipe.

microphone is close to or far from the shell. The only difficulty is that the computation of the external pressure needs the estimation of a Fourier integral that has a slow convergence for a measurement point close to the shell. Then one can do a precise computation around the resonance modes of the shell and a rough one far from these. The interpolation obtained is not very precise but this is not important because the measurements obtained far from the resonance frequencies are noisy. At high frequency, we cannot compare the measurements because the turbulence model is not valid above 3000 Hz. This is due to the problem of spatial resolution of the microphones measuring the wall pressure fluctuations which introduces

a frequency limitation (close to 3500 Hz at 100 m/s) of the turbulence model. It has been necessary to take into account the first nine harmonics. Close to the emergent peaks, the frequency step is 2 Hz while far from these it is 20 Hz. The computation time is about 12 h at 5 mm and 1 h at 20 cm (on a 400 MHz PC).

7. CONCLUSION

In this paper, a comparison between the measured and the computed vibroacoustic response of a baffled cylindrical shell excited by a fully developed turbulent internal flow was presented. The numerical predictions are based, on the one hand, on a theoretical model and, on the other, on an experimental identification of the wall pressure excitation.

The theoretical model gives precise results with a very low computational cost. The composite expansion provides very good results close to the cut-off frequencies of the shell. Obviously, with more complicated geometry or material, the methodology developed here is not applicable but remains useful for a very fast parametric study.

The wall pressure excitation was described by a Corcos-like model which was easily obtained from the measurement of the cross-spectral density of the wall pressure fluctuations. The energetic ($\Phi_p^0(f)$), space ($L_\xi(f)$, $L_\eta(f)$) and convective ($U_c(\xi, f)$) features exhibit standard behaviors for a fully developed turbulent pipe flow.

In conclusion, the results show a very good agreement between the measured and predicted velocity response of the shell. The resonance frequencies were estimated within few percents and the error of the level was limited to 2 dB per third octave. Nevertheless, some points remain to be examined.

Because the extension to the case of heavy fluids is very important from an industrial point of view, it is necessary to verify if the theoretical methodology employed here remains valid for water for instance. Another aspect is that of the influence of the flow on the vibration of the shell. While in air, for Mach numbers less than 0.5, it seems that the flow has little influence, for higher speed flow and heavy fluids, it could be necessary to take it into account.

For the wall pressure excitation, it will be interesting to extend the database to any particular flow velocity owing to non-dimensional representation of the wall pressure characteristics. Moreover, it will be useful to judge the sensitivity of the parameters of the excitation model on the calculated response. Finally, for our configuration, it has been shown that the Corcos-like model describes well the wall pressure excitation. However, we can wonder whether other models [46–48] will give as good results as those obtained here.

ACKNOWLEDGMENT

This work has been supported by the French “Ministère de l’Environnement” (“Réponse vibroacoustique de structures excitées par des écoulements” Convention DGAD/SARE/95104).

REFERENCES

1. M. P. NORTON and M. K. BULL 1984 *Journal of Sound and Vibration* **94**, 105–146. Mechanisms of generation of external acoustic radiation from pipes due to internal flow disturbances.
2. J. M. CLINCH 1970 *Journal of Sound and Vibration* **12**, 429–451. Prediction and measurement of the vibrations induced in thin walled pipes by the passage of internal turbulent water flow.
3. J. HORÁČEK 1986 *Journal Acta Technica ČSAV* **2**, 214–229. The computation of the dynamic response of cylindrical shells in a turbulent flow.
4. W. K. BLAKE 1986 *Mechanics of Flow-induced Sound and Vibration*, Vols. 1 and 2. New York: Academic Press.
5. A. H. NAYFEH 1993 *Introduction to Perturbation Techniques*. New York: John Wiley & Sons.
6. G. A. KRIEGSMANN, A. NORRIS and E. L. REISS 1984 *Journal of the Acoustical Society of America* **75**, 685–694. Acoustic scattering by baffled membranes.
7. A. N. NORRIS 1990 *Journal of Acoustical Society of America* **88**, 505–514. Resonant acoustic scattering from solid targets.
8. H. SCHLICHTING 1960 *Boundary Layer Theory*. New York: McGraw-Hill.
9. G. M. CORCOS 1967 *Journal of Sound and Vibration* **6**, 59–70. The resolution of turbulent pressures at the wall of a boundary layer.
10. J. S. BENDAT and A. G. PIERSOL 1986 *Random Data; Analysis and Measurement Procedures*. New York: Wiley.
11. J. SABOT 1976 *Ph.D. Thesis, Ecole Centrale de Lyon*. Etude de la cohérence spatiale et temporelle de la turbulence établie en conduite.
12. M. K. BULL and Th. LANGEHEINEKEN 1981 *Technical Report 73, Max-Planck-Institut für Stromungsforschung, Gottingen*. On the wall pressure field in turbulent pipe flow.
13. G. F. CAREY, J. E. CHLUPSA and H. H. SCHLOEMER 1967 *Journal of Acoustical Society of America* **41**, 373–379. Acoustic turbulent water-flow tunnel.
14. J. M. CLINCH 1968 *Journal of Sound and Vibration* **9**, 398–419. Measurements of the wall pressure field at the surface of a smooth-walled pipe containing turbulent water flow.
15. V. MASON 1969 *Journal of Sound and Vibration* **10**, 208–226. Some experiments on the propagation of sound along a cylindrical duct containing flowing air.
16. H. M. HELAL, M. J. CASARELLA and T. M. FARABEE 1989 *ASME Winter Annual Meeting, NCA-Vol. 5*, 49–59. An application of noise cancelation techniques to the measurement of wall pressure fluctuations in a wind tunnel.
17. M. P. HORNE and R. J. HANSEN 1981 *Proceedings of the 7th Symposium on Turbulence, University of Missouri, Rolla*, 139–148. Minimization of far field acoustic effects in turbulent boundary layer wall pressure fluctuation experiments.
18. G. C. LAUCHLE and M. A. DANIELS 1987 *Physics of Fluids A, Fluid Dynamics* **30**, 3019–3024. Wall-pressure fluctuations in turbulent pipe flow.
19. R. J. WILSON, B. G. JONES and R. P. ROY 1979 *Proceedings in the 6th Symposium on Turbulence, University of Missouri, Rolla*, 34–45. Measurement techniques of stochastic pressure fluctuations in annular flow.
20. M. P. HORNE and R. A. HANDLER 1991 *Experiments in Fluids* **12**, 136–139. Note on the cancelation of contaminating noise in the measurement of turbulent wall pressure fluctuations.
21. G. M. CORCOS 1963 *Journal of the Acoustical Society of America* **35**, 192–199. Resolution of pressure in turbulence.
22. F. E. CEIB 1969 *Journal of the Acoustical Society of America* **46**, 253–261. Measurements on the effect of transducer size on the resolution of boundary-layer pressure fluctuations.
23. R. M. LUEPTOW 1995 *Journal of the Acoustical Society of America* **97**, 370–378. Transducer resolution and the turbulent wall pressure spectrum.

24. G. SCHEWE 1983 *Journal of Fluid Mechanics* **134**, 311–328. On the structure and resolution of wall-pressure fluctuations associated with turbulent boundary-layer flow.
25. W. W. WILLMARTH and F. W. ROOS 1965 *Journal of Fluid Mechanics* **22**, 81–94. Resolution and structure of the wall pressure field beneath a turbulent boundary layer.
26. T. M. FARABEE and M. J. CASARELLA 1991 *Physics of Fluids A, Fluid Dynamics* **3**, 2410–2420. Spectral features of wall pressure fluctuations beneath turbulent boundary layers.
27. W. L. KEITH, D. A. HURDIS and B. M. ABRAHAM 1992 *Journal of Fluids Engineering* **114**, 338–347. A comparison of turbulent boundary layer wall-pressure spectra.
28. H. P. BAKEWELL, C. F. CAREY, J. J. LIBUHA, H. H. SCLOEMER and W. A. VON WINKLE 1962 *Technical Report 5591-052-00-00, USL, Naval Underwater Systems Center, New London, CT*. Wall pressure correlations in turbulent pipe flow.
29. N. K. AGARWAL 1994 *Journal of Sound and Vibration* **169**, 89–109. The sound field in fully developed turbulent pipe flow due to internal flow separation. Part 1: wall-pressure fluctuations.
30. D. M. CHASE 1987 *Journal of Sound and Vibration* **112**, 125–147. The character of the turbulent wall pressure spectrum at sub-convective wave numbers and a suggested comprehensive model.
31. P. LEEHEY 1988 *Transactions of the ASME, Journal of Vibration, Acoustics, Stress, and Reliability in Design* **110**, 220–225. Structural excitation by turbulent boundary layer: an overview.
32. M. K. BULL 1996 *Journal of Sound and Vibration* **190**, 299–315. Wall-pressure fluctuation beneath turbulent boundary layers: some reflections on forty years of research.
33. W. R. GRAHAM 1997 *Journal of Sound and Vibration* **206**, 541–565. A comparison of models for the wavenumber-frequency spectrum of turbulent boundary layer pressures.
34. B. A. SINGER 1996 *Technical Report 198297, NASA*. Turbulent wall-pressure fluctuations: new model for off-axis cross spectral density.
35. G. ROBERT 1984 *Ph.D. Thesis, Ecole Centrale de Lyon*. Modélisation et simulation du champ exciteur-induit sur une structure par une couche limite turbulente.
36. R. L. PANTON and J. H. LINEBARGER 1974 *Journal of Fluid Mechanics* **65**, 261–287. Wall pressure spectra calculations for equilibrium boundary layers.
37. F. SGARD and N. ATALLA 1997 *Acustica* **83**, 243–250. Mean flow effects on a plate-backed cavity. Part 1: theory. Part 2: results.
38. A. W. LEISSA 1993 *Vibration of Shells*. Acoustical Society of America; originally issued by NASA, 1973.
39. W. FLÜGGE 1973 *Stress in Shells*. Berlin: Springer-Verlag.
40. P. M. MORSE and K. U. INGARD 1968 *Theoretical Acoustics*. New York: McGraw-Hill Book Company.
41. P. M. MORSE and H. FESHBACH 1953 *Methods of Theoretical Physics*. New York: McGraw-Hill Book Company.
42. P. J. T. FILIPPI, A. H. P. VAN DER BURGH, P.-O. MATTEI, C. M. J. DE JONG and C. MAURY 2000 *Journal of Sound and Vibration* **229**, 1157–1169. Sound transmission through a thin baffled plate: validation of a light fluid approximation with numerical and experimental results.
43. P.-O. MATTEI 1995 *Journal of Sound and Vibration* **188**, 111–130. Sound radiation by a baffled shell: comparison of the exact and an approximate solution.
44. R. KRESS 1989 *Linear Integral Equations*. New York: Springer-Verlag.
45. M. ABRAMOWITZ and I. A. STEGUN 1968 *Handbook of Mathematical Functions*. New York: Dover Publications.
46. D. M. CHASE 1980 *Journal of Sound and Vibration* **70**, 29–67. Modeling the wavenumber-frequency spectrum of turbulent boundary layer wall pressure.

- 47. B. M. EFIMTSOV 1982 *Soviet Physics—Acoustics* **28**, 289–292. Characteristics of the field of turbulent wall pressure fluctuations at large Reynolds numbers.
- 48. A. V. SMOL'YAKOV and V. M. TKACHENKO 1991 *Soviet Physics—Acoustics* **37**, 627–630. Model of a field of pseudosonic turbulent wall pressures and experimental data.

APPENDIX A

In this appendix, we give details on the two perturbation expansions used to construct the composite expansion. Let us start from the boundary value problem given by equations (28)–(31) and boundary conditions for the displacement. This system is given by

$$(\bar{C}_c - \rho_c h \omega^2) \bar{u}(Q; Q', \omega) - \begin{pmatrix} 0 \\ 0 \\ p_i^0(Q; Q', \omega) \end{pmatrix} = \begin{pmatrix} 0 \\ 0 \\ \delta_{Q'}(Q) \end{pmatrix}, \quad \begin{cases} Q = (z, \phi, R) \\ Q' = (z', \phi', R) \end{cases} \in \Sigma, \tag{A1}$$

$$\bar{u}(Q; Q', \omega) = \bar{0}, \quad \partial_z u_r(Q; Q', \omega) = 0, \quad Q = (\pm L, \phi, R), \quad Q' = (\pm L, \phi', R), \tag{A2}$$

$$(\Delta + k_i^2) p_i^0(M; M', \omega) = 0, \quad M = (z, \phi, r), \quad M' = (z', \phi', r') \in \Omega_i^0, \tag{A3}$$

$$\partial_r p_i^0(Q; Q', \omega) = \rho_i \omega^2 u_r(Q; Q', \omega), \quad Q = (z, \phi, R), \quad Q'(z', \phi', R) \in \Sigma, \tag{A4}$$

$$\partial_z p_i^0(Q; Q', \omega) \mp \sum_{mn} \psi_{mn}(r, \phi) i \chi_{mn} \int_0^{2\pi} \int_0^R \psi_{mn}^*(r'', \phi'') p_i^0(Q''; Q', \omega) r'' dr'' d\phi'' = 0, \tag{A5}$$

$$Q = (\pm L, \phi, r), \quad Q' = (\pm L, \phi', r'), \quad Q'' = (\pm L, \phi'', r'') \in \sigma^\pm.$$

Equation (A2) represents the boundary condition for a clamped shell [38, 39]. Let $\varepsilon = \rho_i / \rho_c h$, which is a small parameter for a thin steel shell in contact with air.

A.1. OUTER EXPANSION

Far from the cut-off frequencies of the waveguides, the solution of the previous equations is sought as a formal series in ε :

$$\bar{u}^\varepsilon = \bar{U}^0 + \varepsilon \bar{U}^1 + \dots, \quad (p_i^0)^\varepsilon = \Psi^0 + \varepsilon \Psi^1 + \dots.$$

Substituting these two expansions into equations (A1)–(A5), and collecting coefficients of like power of ε on both sides of each equation yields the following.

To order ε^0 ,

$$\left\{ \begin{aligned} (\bar{C}_c - \rho_c h \omega^2) \bar{U}^0(Q; Q', \omega) &= \begin{pmatrix} 0 \\ 0 \\ \delta_{Q'}(Q) \end{pmatrix} + \begin{pmatrix} 0 \\ 0 \\ \Psi^0(Q; Q', \omega) \end{pmatrix}, \quad \begin{cases} Q = (z, \phi, R) \\ Q' = (z', \phi', R) \end{cases} \in \Sigma, \\ \bar{U}^0(Q; Q', \omega) = \bar{0}, \quad \partial_z U_r^0(Q; Q', \omega) = 0, \quad Q = (\pm L, \phi, R), \quad Q' = (\pm L, \phi', R), \\ (\Delta + k_i^2) \Psi^0(M; M', \omega) = 0, \quad M = (z, \phi, r), \quad M' = (z', \phi', r') \in \Omega_i^0, \\ \partial_r \Psi^0(Q; Q', \omega) = 0, \quad Q = (z, \phi, R), \quad Q' = (z', \phi', R) \in \Sigma, \\ \partial_z \Psi^0(Q; Q', \omega) \mp \sum_{mn} \psi_{mn}(r, \phi) i \chi_{mn} \int_0^{2\pi} \int_0^R \psi_{mn}^*(r'', \phi'') \Psi^0(Q''; Q', \omega) r'' dr'' d\phi'' = 0, \\ Q = (\pm L, \phi, r), \quad Q' = (\pm L, \phi', r'), \quad Q'' = (\pm L, \phi'', r'') \in \sigma^\pm; \end{aligned} \right.$$

to order ε^1 ,

$$\left\{ \begin{aligned} (\bar{C}_c - \rho_c h \omega^2) \bar{U}^1(Q; Q', \omega) &= \begin{pmatrix} 0 \\ 0 \\ \delta_{Q'}(Q) \end{pmatrix} + \begin{pmatrix} 0 \\ 0 \\ \Psi^1(Q; Q', \omega) \end{pmatrix}, \quad \begin{cases} Q = (z, \phi, R) \\ Q' = (z', \phi', R) \end{cases} \in \Sigma, \\ \bar{U}^1(Q; Q', \omega) = \bar{0}, \quad \partial_z U_r^1(Q; Q', \omega) = 0, \quad Q = (\pm L, \phi, R), \quad Q' = (\pm L, \phi', R), \\ (\Delta + k_i^2) \Psi^1(M; M', \omega) = 0, \quad M = (z, \phi, r), \quad M' = (z', \phi', r') \in \Omega_i^0, \\ \partial_r \Psi^1(Q; Q', \omega) = \rho_c h \omega^2 U_r^0(Q; Q', \omega), \quad Q = (z, \phi, R), \quad Q' = (z', \phi', R) \in \Sigma, \\ \partial_z \Psi^1(Q; Q', \omega) \mp \sum_{mn} \psi_{mn}(r, \phi) i \chi_{mn} \int_0^{2\pi} \int_0^R \psi_{mn}^*(r'', \phi'') \Psi^1(Q''; Q', \omega) r'' dr'' d\phi'' = 0, \\ Q = (\pm L, \phi, r), \quad Q' = (\pm L, \phi', r'), \quad Q'' = (\pm L, \phi'', r'') \in \sigma^\pm. \end{aligned} \right.$$

Now let Ψ^0 be the solution of

$$\left\{ \begin{aligned} (\Delta + k_i^2) \Psi^0(M; M', \omega) &= 0, \quad M = (z, \phi, r), \quad M' = (z', \phi', r') \in \Omega_i^0, \\ \partial_r \Psi^0(Q; Q', \omega) &= 0, \quad Q = (z, \phi, R), \quad Q' = (z', \phi', R) \in \Sigma, \\ \partial_z \Psi^0(Q; Q', \omega) \mp \sum_{mn} \psi_{mn}(r, \phi) i \chi_{mn} \int_0^{2\pi} \int_0^R \psi_{mn}^*(r'', \phi'') \Psi^0(Q''; Q', \omega) r'' dr'' d\phi'' &= 0, \\ Q = (\pm L, \phi, r), \quad Q' = (\pm L, \phi', r'), \quad Q'' = (\pm L, \phi'', r'') &\in \sigma^\pm, \end{aligned} \right.$$

$\Psi^0(M; M', \omega)$ is the solution of an homogeneous boundary value problem; if the wavenumber k_i is not an eigen-wavenumber, it is obvious that one obtains $\Psi^0(M; M', \omega) = 0, \forall M, M' \in \Omega_i^0$ [40].

Then $\bar{U}^0(Q; Q', \omega)$ is the response of the shell loaded by the external fluid excited by a unit point force, given by

$$\bar{U}^0(Q; Q', \omega) = \bar{\Gamma}_\omega(\bar{e}_r \delta_{Q'}(Q)),$$

where \bar{e}_r is the unit vector normal to the shell and $\bar{\Gamma}_\omega$ is the Green operator of the finite shell loaded by the external fluid (defined for each frequency).

The first order approximation is obtained in a similar way. Let Ψ^1 be the solution of

$$\left\{ \begin{array}{l} (\Delta + k_i^2)\Psi^1(M; M', \omega) = 0, \quad M = (z, \phi, r), \quad M' = (z', \phi', r') \in \Omega_i^0, \\ \partial_r \Psi^1(Q; Q', \omega) = \rho_c h \omega^2 U_r^0(Q; Q', \omega), \quad Q = (z, \phi, R), \quad Q' = (z', \phi', R) \in \Sigma, \\ \partial_z \Psi^1(Q; Q', \omega) \mp \sum_{mn} \psi_{mn}(r, \phi) i \chi_{mn} \int_0^{2\pi} \int_0^R \psi_{mn}^*(r'', \phi'') \Psi^1(Q''; Q', \omega) r'' dr'' d\phi'' = 0, \\ Q = (\pm L, \phi, r), \quad Q' = (\pm L, \phi', r'), \quad Q'' = (\pm L, \phi'', r'') \in \sigma^\pm, \end{array} \right\}.$$

If the wavenumber k_i is not an eigen-wavenumber, one easily can show that

$$\begin{aligned} \Psi^1(M; M', \omega) &= -\rho_c h \omega^2 \int_\Sigma U_r^0(M; Q', \omega) \mathcal{G}_\omega^i(M'; Q') dQ' \\ &= -\rho_c h \omega^2 \sum_{mn} \psi_{mn}(r', \phi') \int_0^{2\pi} \int_{|L}^L U_r^0(z, \phi; z', \phi', \omega) \psi_{mn}^*(R, \phi') \\ &\quad \times \frac{e^{i\chi_{mn}|z-z'|}}{2i\chi_{mn}} R dz' d\phi. \end{aligned} \tag{A6}$$

Now $\bar{U}^1(Q; Q', \omega)$ is the response of the shell loaded by the external fluid excited by a pressure force corresponding to the acoustic pressure radiated in the interior of the waveguide by the shell that has the displacement $\bar{U}^0(Q; Q', \omega)$. That is

$$\bar{U}^1(Q; Q', \omega) = \bar{\Gamma}_\omega(\bar{e}_r \Psi^1(Q; Q', \omega)).$$

It is to be noted that $(p_i^0)^o$ is of order $\mathcal{O}(\varepsilon)$, that is a smaller order effect. But when the amplitude of the shell $\bar{U}^0(Q; Q', \omega)$ becomes important, say at a resonance frequency of the shell loaded by the external fluid, it may be necessary to take into account more terms in the outer expansion. That is, one needs to write

$$\bar{u}^o = \bar{U}^0 + \varepsilon \bar{U}^1 + \varepsilon^2 \bar{U}^2 + \dots, \quad (p_i^0)^o = \Psi^0 + \varepsilon \Psi^1 + \varepsilon^2 \Psi^2 + \dots,$$

where $\Psi^2(M; M', \omega)$ and $\bar{U}^2(Q; Q', \omega)$ are given by

$$\Psi^2(M; M', \omega) = -\rho_c h \omega^2 \int_{\Sigma} U_r^1(M; Q', \omega) \mathcal{G}_{\omega}^i(M'; Q') dQ'$$

$$\bar{U}^2(Q; Q', \omega) = \bar{\Gamma}_{\omega}(\bar{e}_r \Psi^2(Q; Q', \omega)).$$

These terms are given by multi-dimensional integrals and are very expensive to compute. We have not implemented it.

Obviously, when the driving frequency draws near a cut-off frequency of the waveguide, χ_{mn} tends to zero and the integral that appears in equation (A6) is not defined. Then it is necessary to look for an other approximation valid at these frequencies: the inner expansion.

A.2. INNER EXPANSION

Close to the angular frequency $\omega_{pq} = c\kappa_{pq}$, let us define $\omega = \omega_{pq}(1 + \varepsilon^2\alpha)$. α is a tuning parameter measuring the distance from the cut-off frequency. Then one has $\chi_{pq}^2 = \kappa_{pq}^2(1 + \varepsilon^2\alpha^2) - \kappa_{pq}^2 = \kappa_{pq}^2(2\varepsilon^2\alpha + \varepsilon^4\alpha^2)$. Then $\chi_{pq} = \kappa_{pq}\varepsilon\sqrt{2\alpha} + \mathcal{O}(\varepsilon^2)$. χ_{mn} is never equal to zero for all ε . The solution is sought again as a power series of ε :

$$\bar{u}^i = \bar{V}^0 + \varepsilon\bar{V}^1 + \dots, \quad (p_i^0)^i = \hat{\Psi}^0 + \varepsilon\hat{\Psi}^1 + \dots.$$

Again, one substitutes these two expansions into equations (A1–A5). Collecting coefficients of like power of ε on both sides of each equation yields the following.

To order ε^0 ,

$$\left(\begin{array}{l} (\bar{C}_c - \rho_c h \omega_{pq}^2) \bar{V}^0(Q; Q', \omega_{pq}) = \begin{pmatrix} 0 \\ 0 \\ \delta_{Q'}(Q) \end{pmatrix} + \begin{pmatrix} 0 \\ 0 \\ \hat{\Psi}^0(Q; Q', \omega_{pq}) \end{pmatrix}, \quad \begin{cases} Q = (z, \phi, R) \\ Q' = (z', \phi', R) \end{cases} \in \Sigma, \\ \bar{V}^0(Q; Q', \omega_{pq}) = \bar{0}, \quad \partial_z V_r^0(Q; Q', \omega_{pq}) = 0, \quad Q = (\pm L, \phi, R), \quad Q' = (\pm L, \phi', R), \\ (\Delta + k_{ipq}^2) \hat{\Psi}^0(M; M', \omega_{pq}) = 0, \quad M = (z, \phi, r), \quad M' = (z', \phi', r') \in \Omega_i^0, \\ \partial_r \hat{\Psi}^0(Q; Q', \omega_{pq}) = 0, \quad Q = (z, \phi, R), \quad Q' = (z', \phi', R) \in \Sigma, \\ \partial_z \hat{\Psi}^0(Q; Q', \omega_{pq}) \mp \sum_{mn \neq pq} \psi_{mn}(r, \phi) i \chi_{mn} \int_0^{2\pi} \int_0^R \psi_{mn}^*(r'', \phi'') \hat{\Psi}^0(Q''; Q', \omega_{pq}) r'' dr'' d\phi'' = 0, \\ Q = (\pm L, \phi, r), \quad Q' = (\pm L, \phi', r'), \quad Q'' = (\pm L, \phi'', r'') \in \sigma^{\pm}. \end{array} \right.$$

Now let $\tilde{\Psi}$ be the solution of the last three equations of the previous system:

$$\left\{ \begin{aligned} (\Delta + k_{ipq}^2)\tilde{\Psi}^0(M; M', \omega_{pq}) &= 0, \quad M = (z, \phi, r), \quad M' = (z', \phi', r') \in \Omega_i^0, \\ \partial_r \tilde{\Psi}^0(Q; Q', \omega_{pq}) &= 0, \quad Q = (z, \phi, R), \quad Q' = (z', \phi', R) \in \Sigma, \\ \partial_z \tilde{\Psi}^0(Q; Q', \omega_{pq}) \mp \sum_{mn \neq pq} \psi_{mn}^*(r, \phi) i\chi_{mn} \int_0^{2\pi} \int_0^R \psi_{mn}^*(r'', \phi'') \tilde{\Psi}^0(Q''; Q', \omega_{pq}) r'' dr'' d\phi'' &= 0, \\ Q = (\pm L, \phi, r), \quad Q' = (\pm L, \phi', r'), \quad Q'' = (\pm L, \phi'', r'') &\in \sigma^\pm. \end{aligned} \right.$$

$\Psi^0(M; M', \omega)$ is the solution of an homogeneous boundary value problem, if the wavenumber k_i is a simple eigen-wavenumber, it is obvious that one obtains $\Psi^0(z, r, \phi; z', r', \phi', \omega) = A_{pq} \psi_{pq}(r, \phi), \forall M, M'$ where A_{pq} is an undetermined constant. $(p_i^0)^i$ is of order $\mathcal{O}(1)$. It is sufficient to use a zeroth order expansion for the pressure. The displacement is given by

$$V^0(Q; Q', \omega_{pq}) = \bar{\Gamma}_{\omega_{pq}} [\bar{e}_r \delta_{Q'}(Q) + \bar{e}_r A_{pq} \psi_{pq}(Q)].$$

To evaluate the constant A_{pq} , one writes the equation satisfied by $\tilde{\Psi}^1$ which is a homogeneous equation with non-homogeneous boundary conditions on Σ :

$$\left\{ \begin{aligned} (\Delta + k_{ipq}^2)\tilde{\Psi}^1(M; M', \omega_{pq}) &= 0, \quad M = (z, \phi, r), \quad M' = (z', \phi', r') \in \Omega_i^0, \\ \partial_r \tilde{\Psi}^1(Q; Q', \omega_{pq}) &= \rho_c h \omega_{pq}^2 V^0(Q; Q', \omega_{pq}), \quad Q = (z, \phi, R), \quad Q' = (z', \phi', R) \in \Sigma, \\ \partial_z \tilde{\Psi}^1(Q; Q', \omega_{pq}) \mp \sum_{mn \neq pq} \psi_{mn}(r, \phi) i\chi_{mn} \int_0^{2\pi} \int_0^R \psi_{mn}^*(r'', \phi'') \tilde{\Psi}^1(Q''; Q', \omega_{pq}) r'' dr'' d\phi'' &, \\ \mp \psi_{pq}(r, \phi) i\kappa_{pq} \sqrt{2\alpha} \int_0^{2\pi} \int_0^R \psi_{pq}^*(r', \phi') A_{pq} \psi_{pq}(r', \phi') r' dr' d\phi' &= 0, \\ Q = (\pm L, \phi, r), \quad Q' = (\pm L, \phi', r'), \quad Q'' = (\pm L, \phi'', r'') &\in \sigma^\pm. \end{aligned} \right.$$

By using the orthonormality property of the normal modes ψ_{pq} , the second integral of the last equation of the previous system is equal to unity, and then

$$\left\{ \begin{aligned} (\Delta + k_{ipq}^2)\tilde{\Psi}^1(M; M', \omega_{pq}) &= 0, \quad M = (z, \phi, r), \quad M' = (z', \phi', r') \in \Omega_i^0, \\ \partial_r \tilde{\Psi}^1(Q; Q', \omega_{pq}) &= \rho_c h \omega_{pq}^2 V^0(Q; Q', \omega_{pq}), \quad Q = (z, \phi, R), \quad Q' = (z', \phi', R) \in \Sigma, \\ \partial_z \tilde{\Psi}^1(Q; Q', \omega_{pq}) \mp \sum_{mn \neq pq} \psi_{mn}(r, \phi) i\chi_{mn} \int_0^{2\pi} \int_0^R \psi_{mn}^*(r'', \phi'') \tilde{\Psi}^1(Q''; Q', \omega_{pq}) r'' dr'' d\phi'' &, \\ \mp A_{pq} \psi_{pq}(r, \phi) i\kappa_{pq} \sqrt{2\alpha} &= 0, \\ Q = (\pm L, \phi, r), \quad Q' = (\pm L, \phi', r'), \quad Q'' = (\pm L, \phi'', r'') &\in \sigma^\pm. \end{aligned} \right.$$

Classically, this homogeneous Helmholtz equation with non-homogeneous boundary conditions can be brought back to a non-homogeneous Helmholtz equation with homogeneous boundary conditions. Let us define $H(M; M', \omega_{pq})$ as a twice-differentiable function that satisfies

$$\left\{ \begin{aligned} \partial_r H(Q; Q', \omega_{pq}) &= \rho_c h \omega_{pq}^2 V^0(Q; Q', \omega_{pq}), \quad Q = (z, \phi, R), \quad Q' = (z', \phi', R) \in \Sigma, \\ \partial_z H(Q; Q', \omega_{pq}) \mp \sum_{mn \neq pq} \psi_{mn}(r, \phi) i \chi_{mn} \int_0^{2\pi} \int_0^R \psi_{mn}^*(r'', \phi'') \tilde{\Psi}^1(Q''; Q', \omega_{pq}) r'' dr'' d\phi'', \\ &\mp A_{pq} \psi_{pq}(r, \phi) i \kappa_{pq} \sqrt{2\alpha}, \\ Q = (\pm L, \phi, r), \quad Q' &= (\pm L, \phi', r'), \quad Q'' = (\pm L, \phi'', r'') \in \sigma^\pm. \end{aligned} \right.$$

Then $\tilde{\Psi}^1(M; M', \omega_{pq})$ is the solution of

$$\left\{ \begin{aligned} (\Delta + k_{ipq}^2) \tilde{\Psi}^1(M; M', \omega_{pq}) &= -(\Delta + k_{ipq}^2) H(M; M', \omega_{pq}), \quad M = (z, \phi, r), \quad M' = (z', \phi', r') \in \Omega_i^0, \\ \partial_r \tilde{\Psi}^1(Q; Q', \omega_{pq}) &= 0, \quad Q = (z, \phi, R), \quad Q' = (z', \phi', R) \in \Sigma, \\ \partial_z \tilde{\Psi}^1(Q; Q', \omega_{pq}) \mp \sum_{mn \neq pq} \psi_{mn}(r, \phi) i \chi_{mn} \int_0^{2\pi} \int_0^R \psi_{mn}^*(r'', \phi'') \tilde{\Psi}^1(Q''; Q', \omega_{pq}) r'' dr'' d\phi'' &= 0, \\ Q = (\pm L, \phi, r), \quad Q' &= (\pm L, \phi', r'), \quad Q'' = (\pm L, \phi'', r'') \in \sigma^\pm. \end{aligned} \right.$$

To obtain a unique solution to this boundary value problem, the second member of the Helmholtz equation must be orthogonal to the non-trivial solution of the homogeneous problem ψ_{pq} . This solvability condition reads

$$\int_{\Omega_i^0} (\Delta + k_{ipq}^2) H(M; M', \omega_{pq}) \psi_{pq}^*(M) dM = 0.$$

By using Green's theorem, this equation is transformed into

$$\begin{aligned} &\int_{\Sigma} \partial_{\bar{n}_Q} H(Q; M', \omega_{pq}) \psi_{pq}^*(Q) - \partial_{\bar{n}} \psi_{pq}^*(Q) H(Q; M', \omega_{pq}) dQ \\ &+ \int_{\sigma^\pm} \partial_{\bar{n}_Q} H(Q; M', \omega_{pq}) \psi_{pq}^*(Q) - \partial_{\bar{n}} \psi_{pq}^*(Q) H(Q; M', \omega_{pq}) dQ = 0. \end{aligned}$$

Now, applying the boundary conditions, one gets

$$\begin{aligned} &\int_{\Sigma} \rho_c h \omega_{pq}^2 V^0(Q; Q', \omega_{pq}) \psi_{pq}^*(Q) dQ + \int_{\sigma^\pm} \psi_{pq}^*(Q) \{ A_{pq} \psi_{pq}(r, \phi) i \kappa_{pq} \sqrt{2\alpha} \\ &+ \sum_{mn \neq pq} \psi_{mn}(r, \phi) i \chi_{mn} \int_{\sigma^\pm} \psi_{mn}^*(r'', \phi'') H(Q''; Q') dQ'' \} dQ = 0. \end{aligned}$$

By using again the orthonormality property of the normal modes $\psi_{mn}(r, \phi)$, the solvability condition reads

$$\rho_c h \omega_{pq}^2 \int_{\Sigma} V^0(Q; Q', \omega_{pq}) \psi_{pq}^*(Q) dQ + 2A_{pq} i \kappa_{pq} \sqrt{2\alpha} = 0.$$

After a little algebra, one gets the value of A_{pq} defined with finite amplitude for all frequencies:

$$A_{pq} = - \frac{\omega_{pq}^2 \rho_c h \int_{\Sigma} (\bar{\Gamma}_{\omega}(\bar{e}_r \delta_{Q'}(Q)))_r \psi_{pq}(Q)^* dQ}{2i \kappa_{pq} \sqrt{2\alpha} + \omega_{pq}^2 \rho_c h \int_{\Sigma} (\bar{\Gamma}_{\omega}(\bar{e}_r \psi_{pq}(Q)))_r \psi_{pq}(Q) dQ}. \tag{A7}$$